

# **Two-to-One Resonant Multi-Modal Dynamics of Horizontal/Inclined Cables,**

## **Part II: Internal Resonance Activation, Reduced-Order Models and**

### **Nonlinear Normal Modes**

**Narakorn Srinil, Giuseppe Rega**

Department of Structural and Geotechnical Engineering, University of Rome 'La Sapienza',  
via A. Gramsci 53, Rome 00197, Italy

**Abstract.** Resonant multi-modal dynamics due to planar 2:1 internal resonances in the non-linear, finite-amplitude, free vibrations of horizontal/inclined cables are parametrically investigated based on the second-order multiple scales solution in Part I [1]. The already validated kinematically non-condensed cable model accounts for the effects of both non-linear dynamic extensibility and system asymmetry due to inclined sagged configurations. *Actual activation* of 2:1 resonances is discussed, enlightening on a remarkable qualitative difference of horizontal/inclined cables as regards non-linear orthogonality properties of normal modes. Based on the analysis of modal contribution and solution convergence of various resonant cables, hints are obtained on proper *reduced-order model* selections from the asymptotic solution accounting for higher-order effects of quadratic nonlinearities. The dependence of resonant dynamics on coupled vibration amplitudes, and the significant effects of cable sag, inclination and extensibility on system non-linear behavior are highlighted, along with meaningful contributions of longitudinal dynamics. The spatio-temporal variation of non-linear dynamic configurations and dynamic tensions associated with 2:1 *resonant non-linear normal modes* is illustrated. Overall, the analytical predictions are validated by finite difference-based numerical investigations of the original partial-differential equations of motion.

**Key words:** horizontal/inclined sagged cable, internal resonance, higher-order effects, reduced-order models, non-linear normal modes, asymmetry effects

## 1. Introduction

The goal of this paper is to parametrically investigate the multi-modal dynamics due to planar 2:1 internal resonances in the finite-amplitude free vibrations of horizontal/inclined cables based on the approximate closed-form solution obtained by the method of multiple scales (MMS) in Part I [1]. The underlying mechanical formulation is based on the kinematically non-condensed cable model accounting for the effects of both non-linear dynamic extensibility and system asymmetry due to inclined sagged configurations.

The suspended cable, aligned with the global Cartesian co-ordinate system, refers to Figure 1 in Part I [1], with an inclination angle  $\theta$  assigned by keeping the horizontal span  $X_H$  fixed and varying the vertical span  $Y_H$ . The function  $y = y(x)$ , where  $x$  is the spatially independent co-ordinate, describes the cable sagged static equilibrium, and the ensuing planar dynamics about it is described by the coupled longitudinal (horizontal)  $u$  and vertical  $v$  displacements. The dynamic behavior of horizontal/inclined cables is governed by several geometrical and mechanical parameters that can be collected in the unique parameter [2]

$$\lambda/\pi = (1/\pi) \sqrt{(w_C S \cos \theta)^2 EA/T_a^3}, \quad (1)$$

which accounts for also the inclination  $\theta$  effects,  $S$  being the cable equilibrium length,  $E$  the cable Young's modulus,  $A$  its uniform cross-sectional area,  $w_C$  its self-weight per unit unstretched length, and  $T_a$  the static tension at the cable point where the local inclination angle is approximately equal to  $\theta$ . The input values of  $EA$  and  $w_C$  are fixed for a given  $\theta$ , whereas the cable static tension (or its horizontal component  $H$ ) is adjusted to attain the varying  $\lambda/\pi$ , which entails varying values of  $T_a$ ,  $S$ , and cable sag-to-span ratio  $d$ . Following [1], a low-extensible cable with a fixed parameter  $EA/w_C X_H \approx 2580.35$  is analyzed for different  $\theta$  values. Variation of the lowest six planar frequencies  $\omega/\pi$ , non-dimensionalized with respect to the fundamental frequency of the corresponding taut string, is illustrated versus  $\lambda/\pi$  in Figures 1a and 1b for the horizontal ( $\theta = 0^\circ$ ) and inclined ( $\theta = 30^\circ$ ) cables, respectively.

The distinguishing linear dynamic features between horizontal and inclined cables are apparent from Figure 1, namely (i) the modification from crossover (Figure 1a) to avoidance or veering (Figure 1b) phenomenon, and (ii) the associated transition from purely symmetric/anti-symmetric modes to hybrid or asymmetric modes<sup>†</sup>. Amongst other planar (as well as non-planar) internal resonances, nearly tuned planar 2:1 resonances, each one involving the pair of modes ( $r$ ,  $s$ ) indicated along a vertical dotted line, may occur away from (e.g.,  $\lambda/\pi \approx 1.28, 2.95, 3.23$  and  $5.48$ ) crossover/avoidance ( $\lambda/\pi \approx 2n\pi$ ,  $n=1, 2, \dots$ ), whereas nearly tuned planar 1:1 or 2:1 resonances may occur at each crossover/avoidance, involving also out-of-plane modes, thus leading to a multiple internal resonance [3]. Herein, we aim at characterizing the non-linear dynamic features of horizontal/inclined cables away from crossover/avoidance, which are more likely responsible for purely planar resonant dynamics – rarely investigated in the literature –, along with the combined effects of cable sag and inclination. Yet, near-avoidance inclined cables having high modal density will also be analyzed here in order to clarify the strong coupling role of the two coexisting hybrid modes and their significant contribution to system non-linear dynamics.

The paper is organized as follows. In Section 2, the actual activation of planar 2:1 internal resonances in various horizontal/inclined cables is investigated by taking into account the non-linear orthogonality properties of normal modes. The first-order interaction coefficients of different horizontal cable models are also discussed. Then, on accounting for second-order quadratic non-linear effects, a multi-dimensional, resonant/non-resonant, modal contribution analysis of the MMS solution is made in Section 3, and the solution convergence is evaluated in Section 4 in terms of resonantly coupled amplitudes and frequencies. Because the accurate determination of cable non-linear modal shapes is of primary interest from a practical point of view as regards long-term dynamic tension effects, the coupled dynamic configurations of

---

<sup>†</sup> Planar mode shapes in Figure 1 are resolved in the local co-ordinate system, with the displacement being normal to the tangential axis of cable centerline.

resonant non-linear normal modes (NNMs) are determined in Section 5, whereas Section 6 addresses the cable non-linear dynamic tension and its space-time modification. Overall results highlight significant effects of cable sag, inclination and extensibility on system non-linear dynamics. Numerical time histories of the finite difference-based solution, validating the analytical predictions and showing modal interaction features of the original system, are presented in Section 7. The paper ends with a summary and some conclusions. Throughout the paper, reference to Part I [1] is made, where needed, by labeling the relevant Section, Figure, Table and Equation number with the preceding roman ‘I’ symbol.

## 2. Internal Resonance Activation

Actual activation (non-activation) of planar 2:1 resonance involving a high-frequency ( $s$ ) and low-frequency ( $r$ ) mode is governed by the first-order quadratic coefficient  $\mathfrak{R}$  obtained by the MMS, when it is different from (equal to) zero [4]. Based on the kinematically non-condensed model holding for a generic inclined cable, it reads [1]

$$\mathfrak{R} = -2 \int_0^1 \frac{\alpha}{\rho^3} \left\{ \phi'_s \left( \frac{3}{2} \phi'_r \phi''_r + y' \phi'_r \phi'_r + \frac{1}{2} \phi'_r \phi'_r \right) + \phi'_s \left( \frac{y'}{2} \phi'_r \phi'_r + \phi'_r \phi'_r + \frac{3}{2} y' \phi'_r \phi'_r \right) \right\} dx, \quad (2)$$

where a prime denotes differentiation with respect to  $x$ ,  $\rho = \sqrt{1 + y'^2}$ ,  $\alpha = EA/H$ ,  $\phi_m$  and  $\varphi_m$  are the longitudinal and vertical shape functions of the  $m$  ( $m = r, s$ ) planar mode obtained by the Galerkin method using a properly truncated  $N$  sine-based series, see Section I.2.4. To discuss also the strain condensation effects on the resonance activation, we evaluate  $\mathfrak{R}$  with the condensed model of horizontal cable as well,

$$\mathfrak{R} = 2\alpha \left\{ \int_0^1 \varphi_s \varphi_r'' dx \int_0^1 y' \varphi_r' dx + \frac{1}{2} \int_0^1 \varphi_s y'' dx \int_0^1 \varphi_r' \varphi_r' dx \right\}, \quad (3)$$

whose  $\varphi_m$  are available in closed form, see Appendix I.A. The  $\mathfrak{R}$  value in Equations (2) and (3) is seen to depend on the contribution of three factors: the mechanical coefficient  $\alpha$ , the normal modes ( $\phi_m, \varphi_m$ ) and the static shape ( $y', y'', \rho$ ) function, the latter ensuing from Equation I.11 valid for small-sagged arbitrarily inclined cables.

## 2.1 Horizontal Cables

Previous analytical [4] and numerical [5] investigations have shown that a planar 2:1 internal resonance in horizontal cables is not activated when the high-frequency mode is anti-symmetric, even though a 2:1 ( $\omega_s:\omega_r$ ) frequency ratio is satisfied. Such circumstance is herein ensured in Table 1 by the vanishing of  $\mathfrak{R}$  coefficients of both the non-condensed (NC) and condensed (CC) crossover cables ( $\lambda/\pi \approx 2, 4$ ) because of the non-linear orthogonality properties of the anti-symmetric/symmetric (high/low -frequency) modes. On the other hand, due to the involvement of just symmetric high-frequency  $s$  modes for non-crossover ( $\lambda/\pi \approx 1.28, 2.95, 3.23, 5.48$ ) and crossover ( $\lambda/\pi \approx 4$ ) cables (Figure 1a) having different geometrical ( $d$ ) and mechanical ( $\alpha$ ) properties, the 2:1 resonances are activated for both NC and CC models ( $\mathfrak{R} \neq 0$ ), regardless of the low-frequency  $r$  modes being symmetric or anti-symmetric.

To highlight also the  $\rho$ -term effects – already addressed through numerical studies in Section I.5.3 – on the  $\mathfrak{R}$  values of the resonantly activated cables, two NC cases, i.e., with  $\rho \neq 1$  and  $\rho \approx 1$ , are considered. It can be seen that the  $\mathfrak{R}$  values of the NC ( $\rho \approx 1$ ) and CC models are slightly different from each other, whereas the latter differ more significantly from those obtained with the general NC ( $\rho \neq 1$ ) model, notwithstanding the corresponding sag  $d$  values are small for all considered cables (i.e.,  $d < 1:8$ , see [6]).

Generally speaking, these analytical results are in agreement with the numerical results in Section I.5.3, which reveal how accounting ( $\rho \neq 1$ ) or not ( $\rho \approx 1$ ) for the varying  $\rho$ -terms in the approximate PDEs of motion of the NC model entails, at least, quantitative differences in the non-linear dynamic responses, depending on also the system parameters and initial conditions. In turn, the difference between the CC- and NC-based  $\mathfrak{R}$  values stands in the influence of the kinematic condensation procedure applied to the CC model, which essentially neglects the higher-order non-linear effects of longitudinal dynamic deformation on the physics of the problem. Overall, neglecting the longitudinal inertia and the associated coupled displacement

contributions affects the resonance activation only slightly through the  $\Re$  values appearing at the first-order MMS. However, when continuing the MMS analysis to second order, the discrepancies in the quadratic and, especially, cubic coefficients between NC and CC models become outstanding due to the different combination of coupled quadratic/cubic-based coefficients governing various resonant/non-resonant modes (see Table I.3 and Section I.5.4). As a consequence, greater differences may occur. It is also important to remark that the kinematic condensation plays a more pronounced role when considering a larger-sagged or higher-extensible resonant cable [1].

In Figure 2, we show the negligible difference in the  $\varphi_m$  modal shape functions of the NC and CC models through the normalized vertical configurations ( $v_n$ ) of the symmetric 2<sup>nd</sup> ( $r = 2$ ) and 5<sup>th</sup> ( $s = 5$ ) modes of the cables with  $\lambda/\pi \approx 2.95$  (Figures 2a, 2b) and 5.48 (Figures 2c, 2d). Solid (dotted) lines represent NC (CC) results. It is worth noting that, in spite of the apparent opposite phase occurring in  $\varphi_r$  between the two models for  $\lambda/\pi \approx 5.48$  (Figure 2c), there is no sign difference in the associated  $\Re$  values in Table 1. This is because the  $r$ -mode enters Equations (2) and (3) in couple, so that they are independent of the relevant phase change. In contrast, if the phases of the solely-appearing  $s$ -mode of the two models are opposite to each other, a sign difference is expected, which, in turn, could affect the resonant NNMs (Equations I.41-I.45) for given system parameters. Yet, such opposite phase does not affect the sign of second-order quadratic coefficients as the latter, embedded in Equations (I.33)-(I.35), appear in couple.

As the sag  $d$  increases (from .04 to .06) when increasing  $\lambda/\pi$  (from 2.95 to 5.48), the  $|\Re|$  value notably increases, despite the associated  $|\sigma|$  value of frequency detuning ( $\approx |\omega_s - 2\omega_r|$ ) also increases from 0 to .07. In view of Equations (2) and (3), this augmented interaction is due, on one side, to the increasing sag effect, which is a direct consequence of the decreased  $H$  value (and ensuing increased  $\alpha$  value) to attain a greater  $\lambda/\pi$ , on the other side, to the relative changes in the associated static and linear dynamic, mostly vertical, ( $r, s$ ) shape functions (see Figure 2). In addition, a sign difference in  $\Re$  between the two cables is noticeable.

Section I.5.3 has shown how the non-linear planar responses of the approximate NC model with  $\rho \approx 1$  exhibit greater numerical errors, with respect to the exact model, than those of the corresponding NC model with  $\rho \neq 1$ . Moreover, Table 1 exhibits different  $\mathfrak{R}$  values of various NC or CC models, whose differences become much stronger at second order (see, e.g., Table I.3). Accordingly, in order to achieve the most reliable analytical results, the following parametric studies, which are based on the second-order MMS, will rely upon the NC model, with the pertinent non-linear coefficients accounting for the contribution of longitudinal dynamics (no strain condensation) and  $\rho \neq 1$ . In turn, some results based on  $\rho \approx 1$  of the NC model are reported in [7, 8].

## 2.2 Inclined Cables

Consider now inclined cables with the general NC model. The 2:1 resonance activation, with  $\mathfrak{R} \neq 0$ , is nearly always possible in the frequency spectrum (Figure 1b), due to vanishing of the purely symmetric or anti-symmetric spatial character of one of the two (or both) involved modes as a consequence of the asymmetry effects due to inclined sagged configurations. In other words, the non-linear orthogonality properties of normal modes never hold. As an example, the 2:1 resonance involving the high-frequency (asymmetric or hybrid) third (I3) or fourth (I4) mode and the low-frequency first (I1) mode may be activated near second avoidance ( $\lambda/\pi \approx 4$ ), besides those of non-avoidance cables having the same  $\lambda/\pi$  as non-crossover cables (1.28, 2.95, 3.23, 5.48). This is shown in Figures 3a and 3b by the variation versus  $\lambda/\pi$  of the  $|\mathfrak{R}|$  parameters and of the frequency-tuning  $\sigma$  effects, respectively, for the cable with  $\theta = 30^\circ$  and  $N = 15$ .

Inspecting Figure 3, it is found that no perfect tuning ( $\sigma = 0$ ) occurs for the I4-I1 interaction (i.e.,  $\sigma > 0$ ), whereas it occurs near avoidance ( $\lambda/\pi \approx 4.1$ ) for the I3-I1 interaction. All resonant interactions are activated as  $|\mathfrak{R}| \neq 0$ , being relatively high as  $\lambda/\pi$  approaches avoidance. However, when varying  $\lambda/\pi$  farther from avoidance, either to the left ( $\lambda/\pi < 4$ ) for the I3-I1 interaction or to the right ( $\lambda/\pi > 4$ ) for the I4-I1 interaction, the 2:1 resonances may no longer be activated,

despite the non-vanishing  $|\Re|$ . Indeed, being  $\sigma$  significantly different from zero, the frequencies may be far away from proper tuning, consider, e.g., the high values of both  $|\Re| \approx 7729$  (7360) and  $\sigma \approx .5$  (-.5) at  $\lambda/\pi \approx 4.16$  (3.73) for the I4-I1 (I3-I1) interaction. This implies that  $\Re \neq 0$  is a necessary, but not sufficient, condition for such internal resonance to be activated, and that the  $\sigma$  value has also to be accounted for. Regardless of the latter, it is worth noting that the two I3-I1 and I4-I1 interactions involving the same I1 mode yield almost equal values of  $|\Re|$  ( $\approx 5964.018$  and  $5967.215$ ) at  $\lambda/\pi \approx 4.019$ , thus showing the negligible effect of the difference in hybrid shape functions associated with the two coexisting avoidance modes (I3, I4) on the  $|\Re|$  value. However, this effect increases as  $\lambda/\pi$  is far away from avoidance.

In contrast with near-avoidance cables, the  $|\Re|$  values of the I3-I1, I4-I1 interactions progressively decrease – due to decreasing level of “modal hybridity” – as  $\lambda/\pi$  moves towards the right ( $\lambda/\pi \rightarrow \infty$ ) or left ( $\lambda/\pi \rightarrow 2$ ) of second avoidance, respectively, which ultimately reflects the occurrence of a nearly anti-symmetric high-frequency mode.

Overall, the outcomes of the nearly tuned 2:1 resonance activated at second avoidance, irrespective of the involved high-frequency, hybrid, 3<sup>rd</sup> or 4<sup>th</sup> mode, theoretically confirm the numerical results in [9], and enlighten on the distinguishing dynamic behaviors of the second-avoidance cable with respect to those of the second-crossover cable, whose 2:1 resonance is activated only when the high-frequency mode, out of the two coexisting modes, is symmetric [5]. As a general remark, the present analysis gives broad hints about the most likely involvement of a larger number of modes within a multiple internal resonance for avoidance than for crossover cables [e.g., 10, 11], owing to the non-satisfied non-linear orthogonality of the relevant modes.

Some resonant non-avoidance ( $\lambda/\pi \approx 1.28, 2.95, 3.23, 5.48$ ) and near-avoidance ( $\lambda/\pi \approx 3.84, 4.14$ ) inclined cables are given in Table 2, with their properties ( $\theta, d, \alpha, \omega_r, \omega_s$ ) and  $\Re$  values ( $N = 30$ ). The varying  $\theta$  effects ( $\theta = 30^\circ, 45^\circ, 60^\circ$ ) on the resonance activation are also highlighted for  $\lambda/\pi \approx 2.95$ . It is seen that, in comparison with the  $|\Re|$  values in Table 1 for the corresponding



non-crossover cables, those of all non-avoidance cables ( $\theta = 30^\circ$ ) decrease, even though both the sag  $d$  and  $\alpha$  parameters substantially increase. This is likely due to the role played by the inclination  $\theta$ , which, in fact, significantly alters the relative importance of the longitudinal and vertical shape functions affecting the  $\Re$  value. Accordingly, this further decreases as  $\theta$  becomes  $45^\circ$  and  $60^\circ$  for  $\lambda/\pi \approx 2.95$ , consistent with the increasing (absolute) value of  $\sigma$  ( $\approx -.02, -.10, -.24$ ) as  $\theta = 30^\circ, 45^\circ, 60^\circ$ , respectively, which shifts the system dynamics far away from nearly-perfect tuning. Indeed, as displayed in Figure 4, though involving the same resonant modes ( $r = 2, s = 5$ ) for all  $\theta$ , the (normalized)  $u_n$  plays an increasing role with respect to the corresponding  $v_n$  in both the low- (4a, 4c) and high-frequency (4b, 4d) modes as  $\theta$  increases, up to becoming the most significant component. This shows how the cable inclination plays a role in linear dynamics not only as regards the occurrence of asymmetric modes at avoidance, and generally affects the non-linear dynamics up to giving the smallest  $\Re$  value for the maximum  $\theta (60^\circ)$ .

### 3. Resonant/Non-Resonant Quadratic Modal Contributions

Apart from the first-order quadratic coefficient  $\Re$  governing resonance activation, the second-order MMS solution of the coupled amplitudes and frequencies also depend on the second-order coefficients  $K_{rr}$ ,  $K_{ss}$ , and  $K_{rs}$  (Equations (I.33)-(I.35)), which account for the combined effects of quadratic/cubic contributions due to the two resonant (modeled) modes, and for the solely quadratic contributions due to the non-resonant (non-modeled) modes. Thus, prior to evaluating the non-linear dynamic displacement and tension profiles, which are amplitude- and frequency-dependent, it is deemed necessary to examine the quadratic modal contributions responsible for solution convergence. Accordingly, the pertinent percent contributions to each of the quadratic coefficients (labeled  $K_{ii}^Q, i = r, s$ ) are evaluated by considering a finite-dimensional model through which  $M$  is the highest order of retained modes.

The modal contributions for the low- and higher-sagged cables with  $\lambda/\pi \approx 1.28$  ( $r = 1, s = 3, M = 5$ ) and  $5.48$  ( $r = 2, s = 5, M = 15$ ) are considered in Table 3 and 4, respectively, to highlight

the cable sag effects. In each  $\lambda/\pi$  case, the results for  $\theta = 0^\circ$  (Table 1) and  $30^\circ$  (Table 2) are comparatively reported to show the influence of cable inclination. It can be seen that only the non-resonant *symmetric* modes contribute to all coefficients for horizontal (non-crossover) cables [5, 12], whereas *all* non-resonant modes – regardless of their order or spatial character – come into play for inclined cables. This distinctive aspect also holds for the second-order spatial functions of dynamic displacement and velocity (Equations (I.51)-(I.52)). For the cables with  $\lambda/\pi \approx 1.28$ , the quadratic effects due to non-resonant modes, which, in general, can be either positive (softening-type correction) or negative (hardening-type correction), are very small compared with those produced by the two resonant modes ( $> 99\%$ ). Therefore, for these cables, it makes sense to consider a two-degree-of-freedom *reduced-order model* accounting for only the two resonant modes. However, this is not the case for the larger-sagged cables with  $\lambda/\pi \approx 5.48$ , for which the higher-order effects of quadratic nonlinearities become pronounced. As shown in Table 4, a number of non-resonant modes, e.g., the intermediate-order 4<sup>th</sup> (3<sup>rd</sup> and 4<sup>th</sup>) and the higher-order 7<sup>th</sup>, 9<sup>th</sup>, 11<sup>th</sup> (6<sup>th</sup>, 7<sup>th</sup>, 9<sup>th</sup> and 11<sup>th</sup>) modes play a meaningful role, too, in all quadratic coefficients of the horizontal (inclined) cable.

In other cases, some non-resonant modes are seen to play a role even greater than the resonant ones. This may happen, for instance, when the associated  $\lambda/\pi$  values fall in the avoidance zones (Figure 1b), where multiple internal resonances are realized. Consider, e.g., the resonant inclined ( $\theta=30^\circ$ ) cable in Table 2 involving the coupled 1<sup>st</sup> and 4<sup>th</sup> modes or the coupled 1<sup>st</sup> and 3<sup>rd</sup> modes, whose  $\lambda/\pi$  is nearly below ( $\lambda/\pi \approx 3.84$ ) or above ( $\lambda/\pi \approx 4.14$ ) second avoidance, respectively. As shown in Table 5 with  $M = 15$ , the combinations (103.514 %, 94.865 %) of non-resonant modal contributions in the  $K_{rr}^Q$  are greater than those (-3.514 %, 5.135 %) of resonant modal contributions for both  $\lambda/\pi$  (3.84, 4.14), whereas, in the  $K_{rs}^Q$ , the former may be greater than (65.832 %) or nearly equal to (44.038 %) the latter (34.168 % or 55.962 %) for  $\lambda/\pi \approx 3.84$  or 4.14, respectively. As a matter of fact, the major influence substantially results

from the contribution of the 3<sup>rd</sup> (4<sup>th</sup>) hybrid mode which nearly coexists with the 4<sup>th</sup> (3<sup>rd</sup>) one near avoidance at  $\lambda/\pi \approx 3.84$  ( $\lambda/\pi \approx 4.14$ ). Yet, other non-resonant modes, e.g., the intermediate-order 2<sup>nd</sup> and the higher-order 5<sup>th</sup> modes also play a significant role for both  $\lambda/\pi$ , like those in Table 4 for cables with  $\lambda/\pi \approx 5.48$ .

In conjunction with Equations (I.33)-(I.35), these meaningful contributions are due to the associated nearly-vanishing denominators where the difference between squared resonant and non-resonant frequencies appears, as well as to the coupled quadratic terms whose values are non-trivially affected by the asymmetric spatial character of the coexisting hybrid modes. The former are responsible for a multiple resonance condition of near-avoidance cables. Overall, the quadratic modal contributions put into evidence the significance of accounting for both resonant and non-resonant (higher-order) modes in the resonant dynamic solution of cables exhibiting significant sag and/or remarkable asymmetry due to inclination effects. Of course, the higher-order modal contributions become less important when increasing the order of modal truncation up to finally yielding converging results. It is also worth noticing how the resonant two-mode solution, when embedded in an infinite-dimensional Galerkin expansion, is capable of properly signaling the breakdown of the lowest reduced-order modeling. Thus, accounting for also non-resonant modes becomes mandatory.

#### **4. Resonant Non-linear Amplitudes and Frequencies**

The second-order effects on resonant non-linear amplitudes are now investigated, aimed at verifying the solution convergence based on the quadratic modal contributions previously discussed. Equation (I.41) is employed by evaluating the low-frequency  $a_r$  amplitude for given high-frequency  $a_s$  amplitude. Two horizontal non-crossover cables involving different resonant symmetric modes ( $\lambda/\pi \approx 1.28$  and  $2.95$ ) are first considered. Then, to illustrate the asymmetry effects due to the hybrid modes, an inclined near-avoidance cable ( $\theta = 30^\circ$ ,  $\lambda/\pi \approx 4.14$ ) is analyzed. The  $a_s$ - $a_r$  relationships obtained with first-order and  $M$ -varying second-order solutions

are comparatively displayed in Figures 5a, 5b and 5c for  $\lambda/\pi \approx 1.28$  ( $r = 1, s = 3$ ),  $\lambda/\pi \approx 2.95$  ( $r = 2, s = 5$ ) and  $\lambda/\pi \approx 4.14$  ( $r = 1, s = 3$ ), respectively. For the sake of comparison, fixed  $\sigma = 0$  and  $\gamma = \pi$  values are considered, and only stable positive amplitudes according to Equation (I.42) are presented.

Figures 5a and 5b highlight that considering only the first-order term gives considerably overestimated  $a_r$  versus  $a_s$  values with respect to those obtained by second-order solutions. For the low-sagged cable ( $\lambda/\pi \approx 1.28$ ), the second-order amplitude curves, obtained with  $M = R$  (accounting for only the two resonant modes),  $M = 3$  (confirming the no-contribution of the anti-symmetric 2<sup>nd</sup> mode) or  $M = 5$  in Figure 5a, are nearly undistinguishable from each other. Thus, it is definitely reasonable to consider only the minimal (2-DOF) reduced-order resonant model for this cable, because the quadratic effects due to non-resonant modes are negligible. However, as the cable sag increases (Figure 5b,  $\lambda/\pi \approx 2.95$ ), considering only the resonant modes ( $M = R$ ) in the second-order solution entails underestimated  $a_r$  values which, in addition, are limited to a low amplitude  $a_s$  range, due to the rapidly approaching negative value of the resulting term in the bracket of Equation (I.41). The solutions improve and converge at once when considering  $M = 5$ . This means that, since there is no contribution from the anti-symmetric 1<sup>st</sup> and 4<sup>th</sup> modes (see Figure 1a), accounting for only the intermediate symmetric 3<sup>rd</sup> mode is already satisfactory. Of course, in other  $\lambda/\pi \approx 2.95$  cases with  $\theta \neq 0$ , the 1<sup>st</sup> and 4<sup>th</sup> modal contributions are non-trivial. Depending on the symmetric modal interaction, it is also observed that the obtained  $a_r$  amplitudes decrease as the sag or  $\lambda/\pi$  increases for the fixed  $\theta$  and given  $a_s$  amplitudes.

Unlike horizontal cables, the asymmetry effects play a significant role for the near-avoidance cable shown in Figure 5c. The first-order and  $M = R$  second-order solutions yield almost the same  $a_r$  values, which remain unchanged even if accounting for also the 2<sup>nd</sup> mode ( $M = 3$ ). When taking the 4<sup>th</sup> mode – namely, the hybrid non-modeled mode coexisting at second avoidance – into consideration ( $M = 4$ ), the  $a_r$  values considerably increase over the larger  $a_s$  amplitude

range. Eventually, the results converge when  $M = 5$ , confirming the need to consider also some non-resonant higher-order modes in Table 5.

The effects of varying  $\theta$  on both the  $a_r$ - $a_s$  relationship and the backbone curve are now displayed in Figures 6a and 6b, respectively. Since  $\omega_s^{(N)} \approx 2\omega_r^{(N)}$  [1], only the  $r$ -mode non-linear frequency ( $\omega_r^{(N)}$ ) is evaluated through Equation (I.45) and then normalized with respect to the associated linear frequency  $\omega_r$ . With  $\lambda/\pi \approx 2.95$ , the second-order results are shown for the horizontal and inclined ( $\theta = 30^\circ, 45^\circ, 60^\circ$ ) cables with  $M = 5$  and 10, respectively. In view of Figure 6a, the estimated  $a_r$  amplitudes increase as  $\theta$  (as well as the cable sag) increases for given  $a_s$  values, contrary to the case exhibiting the increased sag effects alone (Figures 5b vs 5a). This may be due to exchanged importance of the  $u/v$  shape functions (Figure 4) as  $\theta$  increases, according to which the  $u$  component becomes the dominant contribution to cable response and gives rise to significant changes in the associated non-linear coefficients ( $\mathfrak{R}$ ,  $K_{rr}$ ,  $K_{ss}$ ,  $K_{rs}$ ). As shown in Table 6, the inclination affects both the second-order quadratic ( $K_{ii}^Q$ ) and cubic ( $K_{ii}^C$ ) coefficients, which are of softening-type and hardening-type, respectively. As  $\theta$  increases, all of the absolute summations ( $\Sigma$ ) of quadratic and cubic coefficients decrease, without changing the sign indicating the effective nonlinearity. Evidently, together with the  $\mathfrak{R}$  decrement in Table 2, this entails an overall increment of the estimated  $a_r$  values through Equation (I.41), while keeping  $\sigma$  and  $\gamma$  fixed. Thus, while the backbone curves in Figure 6b exhibit, in general, a hardening behaviour, they become as less hardening as higher  $\theta$  is. This occurs because, as  $\theta$  increases, the softening correction due to the  $a_r$ -dependent term in Equation (I.45) somehow reduces the prevailing hardening corrections due to the first-order (remind that  $\mathfrak{R}$  is positive, while  $\cos\gamma$  is negative) and  $a_s$ -dependent terms. This augmented softening behaviour appears consistent with the effects of the solely increased sag in non-resonant horizontal cables [3].

The effects of varying the cable extensibility  $EA/w_C X_H$  on the resonant amplitudes and  $r$ -mode backbone curve are illustrated in Figures 7a and 7b, respectively, by focusing on

horizontal cables with  $\lambda/\pi \approx 2.95$  ( $N = 30, M = 5$ ). While keeping  $A, w_C$  and  $X_H$  fixed, the  $E$  value (extensibility) is increased (decreased) such that  $EA/w_C X_H \approx 10000, 20000$  with respect to the reference one (2580.35). Meanwhile, in order to maintain  $\lambda/\pi \approx 2.95$  in Figure 1a, the  $H$  and  $T_a$  (sag) values increase (decrease) as  $E$  increases. The assumption of small static strain [1] is still satisfied, and the second-order contributions from the non-resonant 3<sup>rd</sup> mode remain significant. In addition, the absolute values of first-order – as well as second-order ( $\mathfrak{R}$  and  $K_{rr}$  remain positive, while  $K_{ss}$  and  $K_{rs}$  remain negative) – coefficients decrease as  $EA/w_C X_H$  decreases, even though the sag increases. Because of the slight changes in the modal shape functions of low-extensible cables, this decrement is mainly due to the decrement of the pertinent  $\alpha$  ( $=EA/H$ ) parameter, despite  $H$  also decreases. Similar to the increasing  $\theta$  case, the estimated  $a_r$  values increase as the extensibility increases for given  $a_s$ , as shown in Figure 7a. This is a physically expected behaviour because a lower-extensible (e.g., metallic) cable vibrates with smaller amplitudes than a corresponding higher-extensible (e.g., synthetic) cable. Accordingly, the backbone curve in Figure 7b exhibits as more hardening behaviour as lower the extensibility is: this is again expected as the metallic cable is typically stiffer than the synthetic cable. The  $\sigma$  and  $\gamma$  parameter effects on the amplitude/frequency results can be found in [7].

## 5. Resonant NNMs and Their Space-Time Evolution

The second-order effects on the spatial dynamic configurations of the 2:1 resonant NNMs are now illustrated. Three different cables are analyzed in Figures 8a, 8b and 8c, respectively, i.e. the horizontal cable with  $\lambda/\pi \approx 2.95$  and  $a_s = .0002$  (Table 1), and the inclined ( $\theta = 30^\circ$ ) cables (Table 2) far away from avoidances ( $\lambda/\pi \approx 5.48, a_s = .0015$ ) or near second avoidance ( $\lambda/\pi \approx 4.14, a_s = .0003$ ). To gain clear insights into different MMS solutions, the first-order, improved first-order and second-order dynamic configurations (see their definitions in Section I.4.3) of the  $v$  amplitudes (with 51 cable nodes) are comparatively presented with  $\gamma = \pi, \sigma = \beta_{r0} = t = 0$ , the latter value corresponding to zero-velocity configurations, see Equation (I.44).

Overall, it can be seen that significant quantitative (Figures 8a-8c) as well as qualitative (8b and 8c) errors occur when considering the first-order configurations, due to the overestimated (or underestimated)  $a_r$  amplitudes at first order, e.g., in Figures 5a and 5b (or 5c). Thus, it is very important to account for second-order corrections – depending on the non-resonant modes – in both the amplitudes and frequencies. In Figure 8a, quantitative errors are seen to occur also if considering  $M = R$  in the second-order displacement. The results suggest taking the symmetric 3<sup>rd</sup> mode ( $M = 5$ ) into account, consistent with the observation in Figure 5b, the 7<sup>th</sup> mode ( $M = 7$ ) being instead useless. Yet, it is worth noticing how only a small difference occurs between the improved first-order and the second-order configurations with  $M = 5$ , which fully highlights the major importance of accounting for higher-order effects in the amplitude and frequency even in a first-order displacement solution, in order to achieve a reliable NNM. This spatial convergence property also holds when varying the time  $t$ .

In contrast, the importance of accounting for the full second-order analysis (involving also spatial corrections) is apparent in Figures 8b and 8c which refer to the larger-sagged and inclined cables, whose asymmetric features of all superimposed configurations are clearly noticed with respect to the symmetric horizontal cable in Figure 8a. In agreement with Tables 4 and 5, the spatial configurations converge satisfactorily when considering the second-order displacement solution accounting for both resonant/non-resonant modes (e.g.,  $M \approx 7$  in Figure 8b and  $M \approx 5$  in Figure 8c), whereas the improved first-order solution does not converge albeit considering more modes ( $M = 15$  in Figure 8b and  $M = 11$  in Figure 8c). This makes evident that the second-order quadratic nonlinearities are significant for larger-sagged and asymmetric cables, and gives clear hints about the necessity of accounting for also second-order spatial displacement corrections.

Overall, depending on coupled vibration amplitudes, it can be inferred that, in order to obtain reliable reduced-order MMS solutions of the resonant NNMs: (i) Accounting for contributions of non-resonant (higher-order) modes is very important, unless a very low-sagged cable is considered; (ii) it may be sufficient to account for them in the non-linear amplitude and

frequency solutions only, thereby developing an improved first-order displacement solution, for relatively low-sagged cables; (iii) it is necessary to take them into consideration also in the non-linear dynamic displacements (the second-order spatial solution) as the cable sag or inclination effects are significant.

The space-time evolution of the second-order displacements of resonant NNMs is addressed by referring to *both* the  $u$  (dashed lines) and  $v$  (solid lines) components in the analysis over a half non-dimensional  $r$ -mode period  $T_r$  of non-linear oscillation. They are shown in Figures 9a, 9b and 9c, with  $M = 5, 10$  and  $15$ , respectively, for the horizontal and inclined ( $\theta = 45^\circ$ ) cables with  $\lambda/\pi \approx 2.95$ ,  $a_s = .0004$ , and for the inclined ( $\theta = 30^\circ$ ) cable with  $\lambda/\pi \approx 5.48$ ,  $a_s = .001$ . Having in mind the  $u$  and  $v$  modal shapes of the underlying 2<sup>nd</sup> and 5<sup>th</sup> resonant modes for the horizontal and inclined ( $\theta = 45^\circ$ ) cables in Figure 4, an apparently distinctive time-varying non-linear superposition of the two coupled modes is observable in Figures 9a and 9b. Qualitatively, as  $\theta$  increases, the longitudinal amplitudes – which are quite small for the horizontal cable – meaningfully increase, up to becoming comparable with the combined vertical ones, which, in turn, are relatively lower than in the horizontal cable. This visualizes how the longitudinal displacements play an increasingly important role in the non-linear resonant dynamics as  $\theta$  increases for a fixed  $\lambda/\pi$ , and represents a closed-form confirmation of a behavior already exemplified in [9] within a purely numerical solution. Furthermore, a remarkably different time evolution is observed between the symmetric/asymmetric spatial distributions exhibited by the horizontal/inclined cables, respectively.

With a higher number of retained modes and greater amplitudes, the coupled configurations of the inclined cable are likely to exhibit multi-harmonic responses, as shown in Figure 9c whose vertical scales are enlarged with respect to Figures 9a and 9b. This is revealed by the small time-varying local curvatures (e.g., at  $t = .1T_r, .4T_r, .5T_r$ ) due to spatial corrections from higher-order non-resonant modes. The multi-harmonic feature has already been observed through numerical simulations in the vibrations of large-sagged horizontal cables [5].



## 6. Space-Time Modification of Cable Non-Linear Tensions

On accounting for the spatial variation of both static  $e$  and non-linear dynamic  $e_d$  strains, the space-time modification of cable *total tension* can be evaluated through Equation (I.5) with neglected out-of-plane component, wherein the derivatives of the converging second-order  $u$  and  $v$  displacements are calculated through Equation (I.43).  $T_f$  is the non-linear total tension non-dimensionalized with respect to the maximum static tension, which typically takes place at the left support (both supports) for the inclined (horizontal) cable (Figure I.1). Two interesting aspects are emphasized: (i) the inclination effects on the spatial distribution of  $T_f$  response shown in Figure 10a (for cables with  $\lambda/\pi \approx 2.95$ ,  $a_s = .0004$  and  $t = .3T_r$ ); (ii) the space-time  $T_f$  distribution exhibiting the strain variation effects shown in Figure 10b (for the inclined cable with  $\theta = 30^\circ$ ,  $\lambda/\pi \approx 5.48$ ,  $a_s = .001$ ,  $t = 0-.5T_r$ ). Again, the prescribed values  $\gamma = \pi$ ,  $\sigma = \beta_{r0} = 0$  are assigned in all cases.

Figure 10a clearly shows that, while the spatially symmetric  $T_f$  response of the horizontal cable exhibits a limited variation along the cable span-length, the spatially unsymmetrical  $T_f$  responses of all inclined cables (see also Figure 9b for  $\theta = 45^\circ$ ) markedly diminish (non-linearly) as one moves towards the right support or as  $\theta$  increases. This entails a meaningful difference between the maximum/minimum total tensions, which increases with  $\theta$  [9], and implies that, during non-linear vibrations, the resulting total tension at any cable point is smaller than the initial maximum static tension due to a negative oscillation-induced tension. Accordingly, the non-linearity produces a less-hardening behavior of higher-inclined cables, as already observed in Figure 6b. From the engineering viewpoint, special care has to be paid to the possibility of cable loosening [13] at the lower-right end support as  $\theta$  increases (see, e.g., Figure 10a,  $\theta = 60^\circ$ ), this being one major design aspect. Yet, also the maximum  $T_f$  taking place at the left-end support for all  $\theta$  must be properly considered by looking at the relevant time history. As an example, this is reported in Figure 11 for the horizontal cable in Figure 9a, along with the  $T_f$  time histories at other positions, i.e., at 1/8, 1/4 and middle span. It is seen that all periodic  $T_f$  responses become

considerably greater or smaller than their initial estimated values, with the left-support tension still exhibiting the maximum value, whereas the mid-span tension exhibiting the minimum one. Consequently, the time-varying difference between maximum/minimum tensions becomes appreciable at a specific time, highlighting that the usual strain condensation model assuming spatially-uniform dynamic tension is no more suitable for such small-sagged cable exhibiting internal resonance.

In Figure 10b, the overall space-time variability of tension response becomes even more apparent for the inclined and larger-sagged cable, where the spatially non-uniform and non-symmetric features are seen to entail the occurrence of the largest or smallest values of total tension along time evolution, also at cable positions other than the supports: see, e.g., the distributed tension peaks occurring at  $t = 0$  or  $.5T_r$ , and their associated configurations in Figure 9c. All of these results confirm the advantage of making use of the non-condensed model which properly accounts for the spatial variability of non-linear dynamic strain, in order to ascertain the actual extreme values of total tension response.

## 7. Modal Interaction Features: Numerical Validation of Analytical Predictions

The analytical MMS predictions are now validated by numerical results. Instead of integrating the system ODEs (I.17) with a prescribed number of modes, the space-time finite difference method (FDM), coupled with a predictor-corrector iteration [5, 7], is directly applied to the original PDEs (I.53-I.54) neglecting the out-of-plane component, to determine the actual dynamic responses under specified initial conditions. To this end, the responses are initiated by the associated coupled displacements (Equation I.43) and velocities (Equation I.44). In the following, the non-dimensionalized responses are plotted against the time parameter  $T$  obtained by non-dimensionalizing the physical time with respect to the  $r$ -mode natural period.

In the spatial convergence background of different MMS solutions reported in Figure 8a for the horizontal cable with  $\lambda/\pi \approx 2.95$  and  $t = 0$ , the numerical  $v$  responses at 1/8 span (node 6),

obtained with the  $u$ ,  $v$  initial displacement conditions of first-order, improved first-order and second-order configurations are comparatively illustrated in Figure 12. Depending on the obtained  $a_r$  amplitudes for the specified  $a_s = .0002$  (Figure 5b), it can be seen that all responses show the periodically-modulated interaction features due to the 2:1 resonance, but some of them differ in both the extent and duration of the modulation, see the first-order (Figure 12a), improved first-order with  $M = 5$  (Figure 12b) and second-order with  $M = R$  (Figure 12c) time histories. Yet, the modulation feature in the response initiated by the improved first-order solution (Figure 12b) is practically similar to those in the responses initiated by the second-order solutions with  $M = 5$  (solid lines) or 10 (circles) in Figure 12d. This highlights, with regard to the temporal aspect, both the possibility of considering just the improved first-order solution and the convergence properties of the second-order spatial solution, already observed in the analytical framework. This holds also for the corresponding inclined cable which exhibits equally comparable FDM time laws as the present horizontal cable [8]. Of course, the amplitude modulations characterizing the actual resonant interaction in Figure 12 initiated by the coupled-mode displacements are substantially different from those initiated by the single-mode ones in Figure I.7. On the other hand, they do not occur in the periodic time laws corresponding to the stationary amplitude MMS solutions.

Moving to various inclined cables with  $\lambda/\pi \approx 2.95$  and larger  $a_s = .0004$  (corresponding to Figure 6), meaningful differences in terms of extent and duration of resonant modal interactions are noticeable in the  $u$  (solid lines) and  $v$  (dashed lines) responses at 1/8 span shown in Figure 13, which are initiated with the second-order  $u$  and  $v$  displacements at  $t = 0$ . With respect to Figure 12d for the horizontal cable with  $a_s = .0002$  and  $a_r \approx .00023$  (Figure 6a), the horizontal cable response in Figure 13a has a longer modulation due to the relatively different contribution of the lower  $a_r \approx .00018$ : this reflects the amplitude-dependence of system resonant dynamics into the time law. Apart from the considerable increment (decrement) in the  $u$  ( $v$ ) response – as well as in the  $a_r$  amplitudes in Figure 6a – as  $\theta$  increases, the maximum inclined cable with  $\theta =$

60° (Figure 13d) exhibits the shortest modulation. This highlights the inclination effects on the non-linear temporal features of the original system. The Fourier amplitude spectral densities (PSDs) of the  $v$  responses in Figure 13 are also reported in Figure 14, all of them clearly revealing two major frequencies. This property and the observed beating-type energy transfer due to modal interaction confirm the theoretical prediction about activation of the planar 2:1 resonance involving just the modeled 2<sup>nd</sup> and 5<sup>th</sup> modes of non-crossover/non-avoidance cables.

With the second-order MMS initial displacement conditions at  $t = 0$ , the numerical FDM  $v$  responses (at node 6) showing the effects of varying the given  $a_s$  amplitude, or the angle  $\theta$ , or the extensibility  $E$  on the response of cables with  $\lambda/\pi \approx 2.95$  are summarized in Figures 15a-15c, respectively, also to the aim of validating the non-linear behaviors predicted by the MMS solution. For a fixed  $\theta$ , i.e. for the horizontal cable, Figure 15a shows that (i) the system responses are as more hardening as greater  $a_s$  is, in agreement with Figure 6. In turn, when varying the angle  $\theta$  for a fixed  $a_s = .0004$ , (ii) the responses in Figure 15b reflect the less-hardening non-linearity as  $\theta$  increases, again in agreement with Figure 6. Moreover, when varying the extensibility for fixed  $\theta = 0^\circ$  and  $a_s = .0002$  values, (iii) the response in Figure 15c is seen to be as more hardening as higher the parameter  $EA/W_c X_H$  is, in agreement with Figure 7. Hence, overall analytical predictions are validated by numerical FDM results.

Next, it is interesting to evaluate how the non-linear resonant response evolves when initiating both the spatial displacement and velocity fields of second-order MMS solution, with respect to that initiated by zero-velocity ( $t = 0$ ) displacements. For this purpose, two initial  $u, v$  conditions are considered: one corresponding to the MMS displacements at  $t = 0$ ; the other corresponding to the MMS displacements/velocities at  $t = .3T_r$ . The associated FDM  $u$  responses at various positions, including nodes 6 (solid lines), 12 (open circles), 26 (dashed lines) and 42 (dotted lines), are comparatively shown in Figures 16a and 16b, respectively, for the inclined cable with  $\theta = 60^\circ$ ,  $\lambda/\pi \approx 2.95$  and  $a_s = .00026$ . Obviously, though initiated with different amplitudes, phases and velocities, the response at each position exhibits the same qualitative

behavior in both figures regarding the extent and duration of the resonantly periodic modulation, which, indeed, holds true also for other inclined cables. Thus, the characterizing amplitude-modulated response of the original system is shown to be invariant with respect to the stationary MMS displacements and/or velocities entering the initial conditions. In addition, the numerical results confirm that, apart from the distinctive extent of modulation, the duration of modal interaction is the same at different cable positions.

Finally, the amplitude modulation features of the non-dimensional FDM-based displacement and velocity are illustrated through the phase portraits in Figures 17a (1/8 span), 17b (1/4 span) and 17c (mid-span) against the corresponding stationary MMS-based portraits in Figures 17d, 17e and 17f, respectively, for the horizontal cable with  $\lambda/\pi \approx 2.95$  and  $a_s = .0002$  under initial conditions of the second-order MMS at  $t = .3T_r$ . Besides confirming the different extent of amplitude modulation occurring at different cable positions, the overall similarity between non-stationary (FDM) and stationary (MMS) phase portraits is highlighted, with the mid-span response exhibiting the largest portrait and modulation.

## 8. Summary and Conclusions

Based on the kinematically non-condensed cable model accounting for the effects of both non-linear dynamic extensibility and system asymmetry due to inclined sagged configurations, planar 2:1 *resonant multi-modal* non-linear free vibrations of horizontal/inclined cables have been investigated through the second-order multiple scales solution obtained in Part I [1]. The main features of the parametric analysis are summarized as follows.

(i) *Internal resonance activation* has been discussed through the interaction coefficients, distinguishing the dynamic characteristics of horizontal/inclined cables as regards the non-linear orthogonality properties of normal modes. For horizontal cables, the internal resonance is always activated when the involved high-frequency mode is symmetric, whereas, owing to the asymmetry effects of inclined configurations entailing *modal hybridity*, the resonance activation

in inclined cables is nearly always possible – depending on frequency-tuning and hybridity capacity – and occurs over a wide range of system parameters.

(ii) Based on a multi-dimensional Galerkin discretization, analysis of second-order quadratic modal contributions has shown that, besides the two resonant modes, *only symmetric* non-resonant modes affect the solution of (non-crossover) horizontal cables, whereas *all* non-resonant modes – irrespective of their order or spatial character – do contribute for inclined cables. Moreover, some non-resonant modes may play a role even greater than the resonant ones. This occurs, for instance, in the avoidance zone of the frequency spectrum wherein, due to the system high modal density and strong coupling, the non-modeled hybrid mode – out of the two coexisting at avoidance – contributes to the response greater than the directly-modeled hybrid mode. This highlights the necessity of accounting for both of them and the possible involvement of a larger number of coupled modes in avoidance cables than in crossover cables.

(iii) As regards the *reduced-order modeling* issue, the convergence studies accounting for higher-order effects of quadratic nonlinearities on non-linear amplitudes, frequencies and dynamic configurations of the resonant NNMs have indicated that, depending on the system parameters and coupled amplitudes, the contributions of *non-resonant* (higher-order) modes are very important. The minimal (two-degree-of-freedom) model involving only the *resonant* modes shows capable of providing reliable results only for a very low-sagged cable. In turn, it may be sufficient to account for non-resonant modes in the non-linear amplitudes and frequencies only, thereby developing an improved first-order solution, for relatively low-sagged cables; otherwise, they should be accounted for also in the dynamic displacements (the full second-order solution) as the cable sag and/or inclination (asymmetry) becomes significant.

(iv) A qualitative difference in the symmetric/asymmetric spatial distribution of the time-varying superimposition of the two resonant modes between horizontal/inclined cables has been highlighted, showing also the meaningful role of *longitudinal displacement* dynamics as cable

inclination increases, and the *multi-harmonic* response features owed to higher-order non-resonant modes for inclined sagged cables.

(v) The *spatio-temporal variability* of non-linear dynamic tension has been presented, emphasizing the importance of accounting for spatial variation of cable non-linear strain through the non-condensed model since appreciable time-varying differences between maximum/minimum total tensions occur even in shallow horizontal cables.

Overall, significant effects of cable sag, inclination, extensibility as well as longitudinal displacements on the non-linear resonant dynamics have been evidenced. Moreover, *finite difference* displacement time laws obtained from the original partial-differential equations of motion have confirmed the predictions and the amplitude-dependent properties of the *multiple scales* solution, by also showing periodically modulated interaction features.

Apart from making available the approximate general non-condensed model valid for horizontal/inclined sagged cables, and for showing its thorough accuracy with respect to the exact model in Part I [1], the comprehensive analysis of resonant *non-linear normal modes* has provided worthwhile information as regards deriving accurate reduced-order cable models and qualifying the non-linear dynamic properties of horizontal/inclined cables to be properly recognized within an upcoming forced vibration analysis.

### **Acknowledgements**

Dr. Narakorn Srinil would like to express his gratitude to the support of the University of Rome ‘La Sapienza’, Italy, through a *Postdoctoral Research Fellowship*.

### **References**

1. Srinil, N., Rega, G., and S. Chucheepsakul, ‘Two-to-one resonant multi-modal dynamics of horizontal/inclined cables. Part I: Theoretical formulation and model validation’, *Nonlinear Dynamics*, 2005, submitted for publication.

2. Triantafyllou, M. S., and Grinfogel, L., 'Natural frequencies and modes of inclined cables', *ASCE Journal of Structural Engineering* **112**, 1986, 139-148.
3. Rega, G., 'Nonlinear dynamics of suspended cables. Part II: Deterministic phenomena', *ASME Applied Mechanics Reviews* **57**, 2004, 479-514.
4. Lacarbonara, W., and Rega, G., 'Resonant nonlinear normal modes. Part II: Activation/orthogonality conditions for shallow structural systems', *International Journal of Non-linear Mechanics* **38**, 2003, 873-887.
5. Srinil, N., Rega, G. and Chucheepsakul, S., 'Three-dimensional nonlinear coupling and dynamic tension in the large amplitude free vibrations of arbitrarily sagged cables', *Journal of Sound and Vibration* **269**, 2004, 823-852.
6. Irvine, H. M., and Caughey, T. K., 'The linear theory of free vibrations of a suspended cable', *Proceeding of the Royal Society of London Series A* **341**, 1974, 229-315.
7. Srinil, N., 'Large-amplitude three-dimensional dynamic analysis of arbitrarily inclined sagged extensible cables', Ph.D. Dissertation, King Mongkut's University of Technology Thonburi, Bangkok, Thailand, 2004.
8. Rega, G., Srinil, N., and S. Chucheepsakul, 'Internally resonant nonlinear free vibrations of horizontal/inclined sagged cables', in *Proceeding of the 5th International Conference on Multibody Systems, Nonlinear Dynamics, and Control*, California, USA, DETC2005-84752, 2005.
9. Srinil, N., Rega, G., and Chucheepsakul, S., 'Large amplitude three-dimensional free vibrations of inclined sagged elastic cables', *Nonlinear Dynamics* **33**, 2003, 129-154.
10. Rega, G., Lacarbonara, W., Nayfeh, A. H., and Chin, C. M., 'Multiple resonances in suspended cables: Direct versus reduced-order models', *International Journal of Non-linear Mechanics* **34**, 1999, 901-924.
11. Nayfeh, A. H., Arafat, H. N., Chin, C. M., and Lacarbonara, W., 'Multimode interactions in suspended cables', *Journal of Vibration and Control* **8**, 2002, 337-387.



12. Arafat, H. N., and Nayfeh, A. H., ‘Non-linear responses of suspended cables to primary resonance excitations’, *Journal of Sound and Vibration* **266**, 2003, 325-354.
13. Wu, Q., Takahashi, K., and Nakamura, S., ‘Non-linear vibrations of cables considering loosening’, *Journal of Sound and Vibration* **261**, 2003, 385-402.

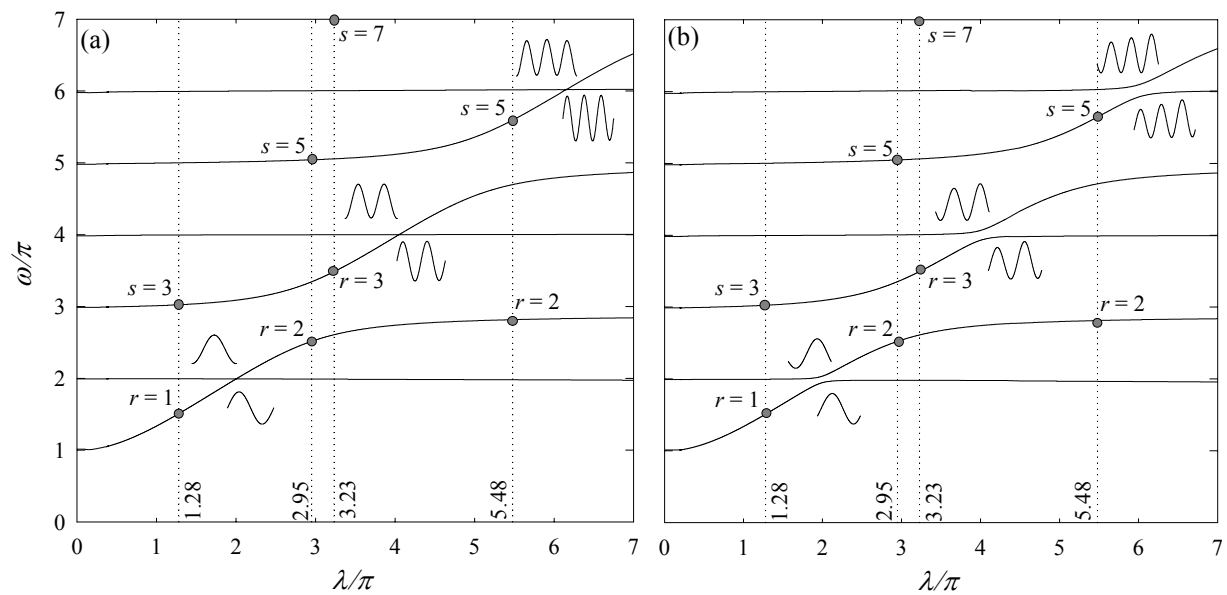
### List of Figures

Figure	Page
1 Crossover (symmetric/anti-symmetric) and avoidance (hybrid) phenomena (modes) in natural frequency spectrum of (a) horizontal and (b) inclined ( $\theta = 30^\circ$ ) cables, with pairs ( $r, s$ ) of 2:1 resonant modes (vertical dotted lines) for non-crossover and non-avoidance cables.	28
2 Vertical $v_n$ components of 2 <sup>nd</sup> and 5 <sup>th</sup> modes for horizontal cables with $\lambda/\pi \approx 2.95$ (a, b) and $\lambda/\pi \approx 5.48$ (c, d): solid (dotted) lines refer to NC (CC) model.	29
3 Variation of (a) $ \Re $ and (b) $\sigma$ versus $\lambda/\pi$ around second avoidance in 2:1 resonance case involving third (I3) and first (I1) modes (solid lines) or fourth (I4) and first (I1) modes (dashed lines), for inclined cable with $\theta = 30^\circ$ .	30
4 Longitudinal $u_n$ (a, b) and vertical $v_n$ (c, d) components of 2 <sup>nd</sup> and 5 <sup>th</sup> modes for various inclined cables having $\lambda/\pi \approx 2.95$ : dashed (dotted, dashed-dotted, solid) lines denote $\theta = 0^\circ$ ( $\theta = 30^\circ, 45^\circ, 60^\circ$ ).	31
5 Resonant $a_s$ - $a_r$ amplitudes for different MMS solutions: (a) $\theta = 0^\circ$ , $\lambda/\pi \approx 1.28$ ; (b) $\theta = 0^\circ$ , $\lambda/\pi \approx 2.95$ ; (c) $\theta = 30^\circ$ , $\lambda/\pi \approx 4.14$ .	32
6 Cable inclination effects on (a) resonant $a_s$ - $a_r$ amplitudes and (b) $r$ -mode backbone curve for various inclined cables with $\lambda/\pi \approx 2.95$ .	33
7 Cable extensibility effects on (a) resonant $a_s$ - $a_r$ amplitudes and (b) $r$ -mode backbone curve for horizontal cables with $\lambda/\pi \approx 2.95$ .	33
8 Different first-order and second-order MMS $v$ displacements of non-linear dynamic configurations for horizontal cable with (a) $\lambda/\pi \approx 2.95$ , $a_s = .0002$ and inclined ( $\theta = 30^\circ$ ) cables with (b) $\lambda/\pi \approx 5.48$ , $a_s = .0015$ and (c) $\lambda/\pi \approx 4.14$ , $a_s = .0003$ .	34
9 Comparison of space-time second-order $u$ (dashed lines) and $v$ (solid lines) components of resonant NNMs over a half non-linear period $T_r$ : (a) $\theta = 0^\circ$ ,	35

- $\lambda/\pi \approx 2.95$ ,  $a_s = .0004$ ; (b)  $\theta = 45^\circ$ ,  $\lambda/\pi \approx 2.95$ ,  $a_s = .0004$ ; (c)  $\theta = 30^\circ$ ,  $\lambda/\pi \approx 5.48$ ,  $a_s = .001$ .
- 10 Spatially non-uniform total tension responses: (a) cables with  $\lambda/\pi \approx 2.95$ ,  $a_s = .0004$  and  $t = 0.3T_r$ ; (b) inclined ( $\theta = 30^\circ$ ) cable with  $\lambda/\pi \approx 5.48$ ,  $a_s = .001$  and  $t = 0-0.5T_r$ . 36
- 11 Total tension responses at different cable positions for horizontal cable with  $\lambda/\pi \approx 2.95$  in Figure 9a. 36
- 12 FDM-based time laws of  $v$  component at 1/8 span for horizontal cable with  $\lambda/\pi \approx 2.95$  and  $a_s = .0002$ , under different initial conditions associated with MMS solutions: (a) first order, (b) improved first order with  $M=5$ , (c) second order with  $M=R$ , (d)  $M=5$  (solid line) and  $M=10$  (circles). 37
- 13 Cable inclination effects on FDM-based time laws of  $u$  (solid lines) and  $v$  (dotted lines) components at 1/8 span for cables with  $\lambda/\pi \approx 2.95$  and  $a_s = .0004$ , under second-order MMS initial displacements: (a)  $\theta = 0^\circ$  with  $M=5$ ; (b)  $\theta = 30^\circ$ , (c)  $\theta = 45^\circ$  and (d)  $\theta = 60^\circ$  with  $M=10$ . 38
- 14 Fourier amplitude spectral densities associated with  $v$  responses in Figure 13: a)  $\theta = 0^\circ$ ; (b)  $\theta = 30^\circ$ , (c)  $\theta = 45^\circ$  and (d)  $\theta = 60^\circ$ . 39
- 15 Effects of varying parameters on system non-linear behavior of cables with  $\lambda/\pi \approx 2.95$  through FDM time laws: varying (a)  $a_s$  for  $\theta = 0^\circ$ , (b)  $\theta$  for  $a_s = .0004$ , (c)  $EA/W_C X_H$  for  $\theta = 0^\circ$  and  $a_s = .0002$ . 40
- 16 FDM-based time laws of  $u$  component at various cable positions for inclined ( $\theta = 60^\circ$ ) cable with  $\lambda/\pi \approx 2.95$  and  $a_s = .00026$ , under second-order MMS (a) initial displacements at  $t = 0$  and (b) initial displacements and velocities at  $t = .3T_r$ : nodes 6 (solid lines), 12 (open circles), 26 (dashed lines) and 42 (dotted lines). 41
- 17 FDM-based (a, b, c) and MMS-based (d, e, f) phase portraits of  $v$  component at different cable positions (1/8, 1/4 and middle span) for horizontal cable with  $\lambda/\pi \approx 2.95$  and  $a_s = .0002$ , under second-order MMS initial displacements and velocities at  $t = .3T_r$ . 42

## List of Tables

<b>Table</b>		<b>Page</b>
1	Cable properties and $\Re$ values with NC ( $N = 30$ ) and CC models for different resonant/non-resonant horizontal cables.	43
2	Cable properties and $\Re$ values by NC model ( $N = 30$ ) for different resonant inclined cables.	43
3	Second-order quadratic modal contributions for horizontal and inclined ( $\theta = 30^\circ$ ) cables with $\lambda/\pi \approx 1.28$ , $N = 30$ and $M = 5$ .	44
4	Second-order quadratic modal contributions for horizontal and inclined ( $\theta = 30^\circ$ ) cables with $\lambda/\pi \approx 5.48$ , $N = 30$ and $M = 15$ .	44
5	Second-order quadratic modal contributions for inclined ( $\theta = 30^\circ$ ) cables near second avoidance: (a) $\lambda/\pi \approx 3.84$ and (b) $\lambda/\pi \approx 4.14$ , with $N = 30$ and $M = 15$ .	44
6	Second-order quadratic and cubic coefficients of various inclined cables with $\lambda/\pi \approx 2.95$ , $N = 30$ and $M = 10$ : (a) $K_{rr}$ , (b) $K_{ss}$ , (c) $K_{rs}$ .	45



**Figure 1**

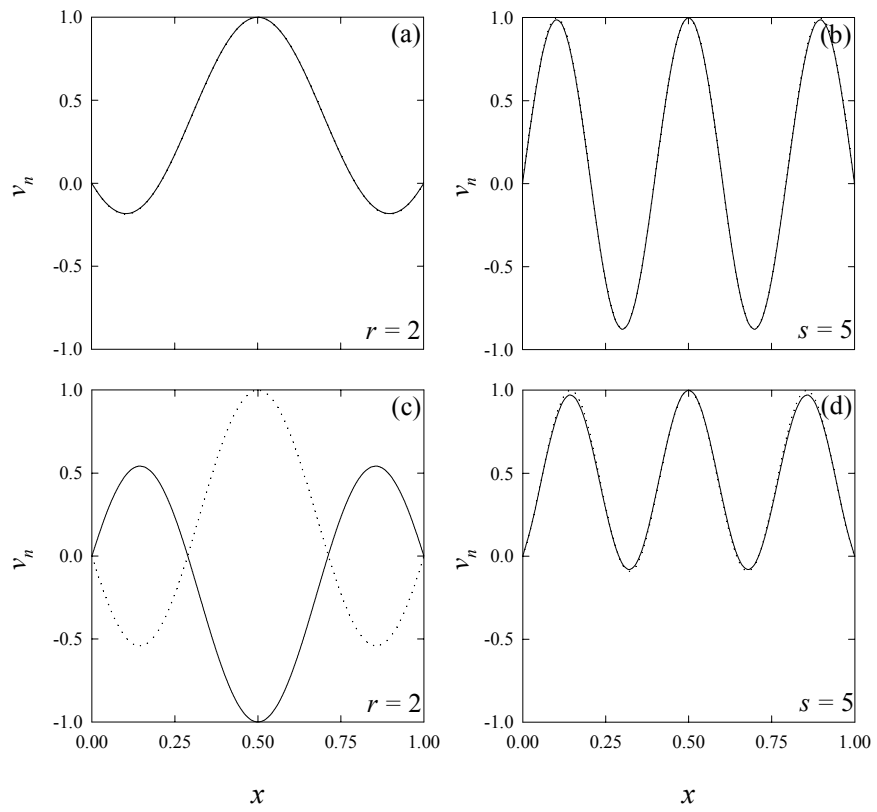


**Figure 2**

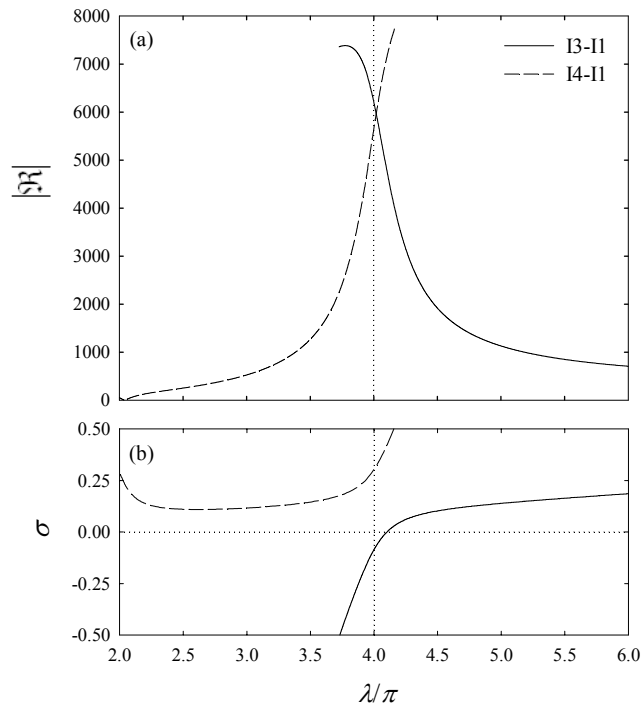


**Figure 3**

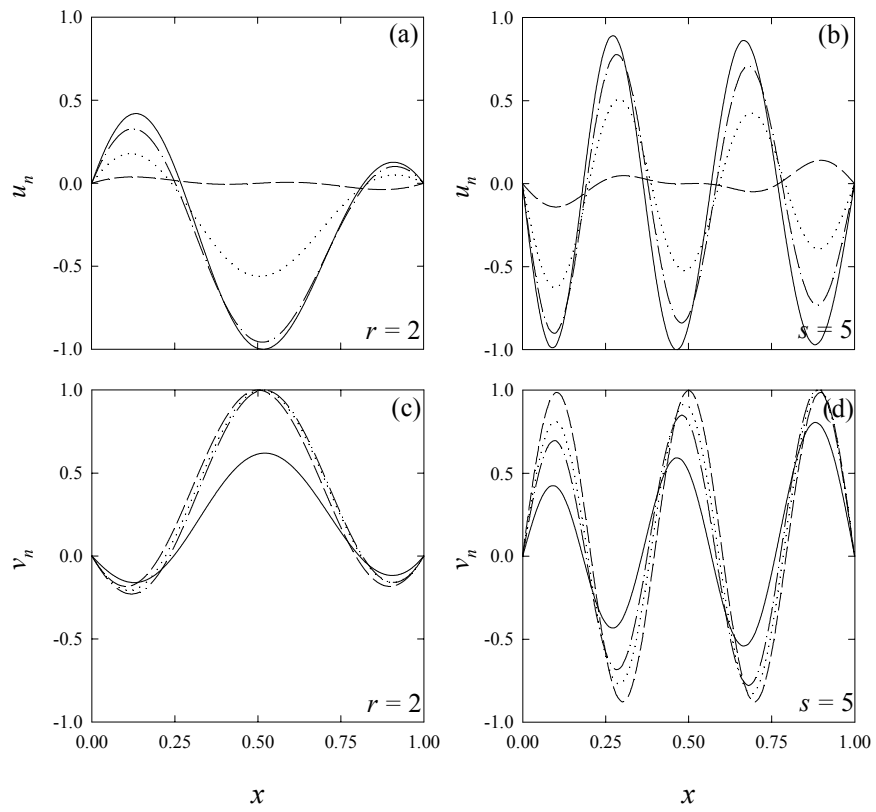


**Figure 4**

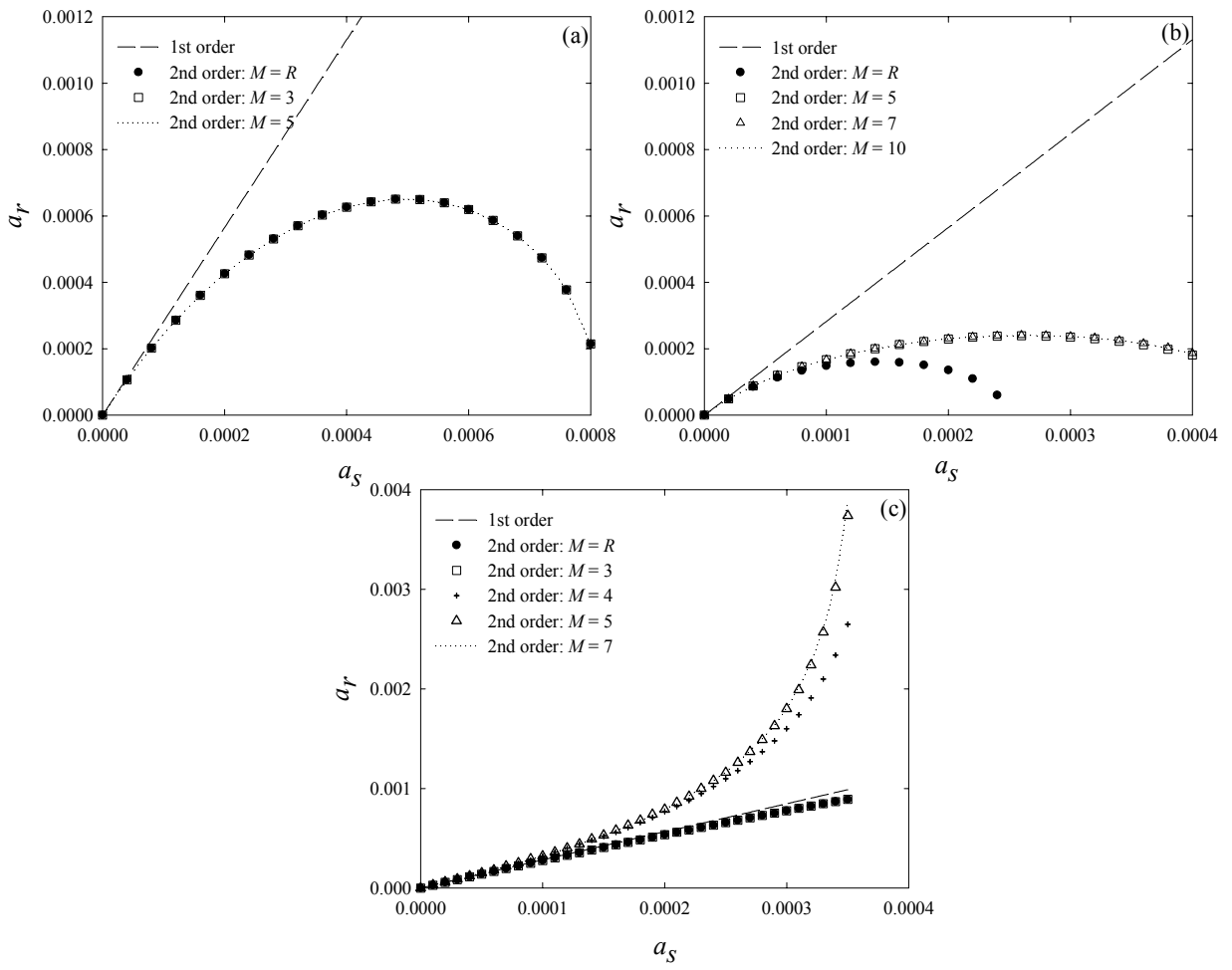


**Figure 5**



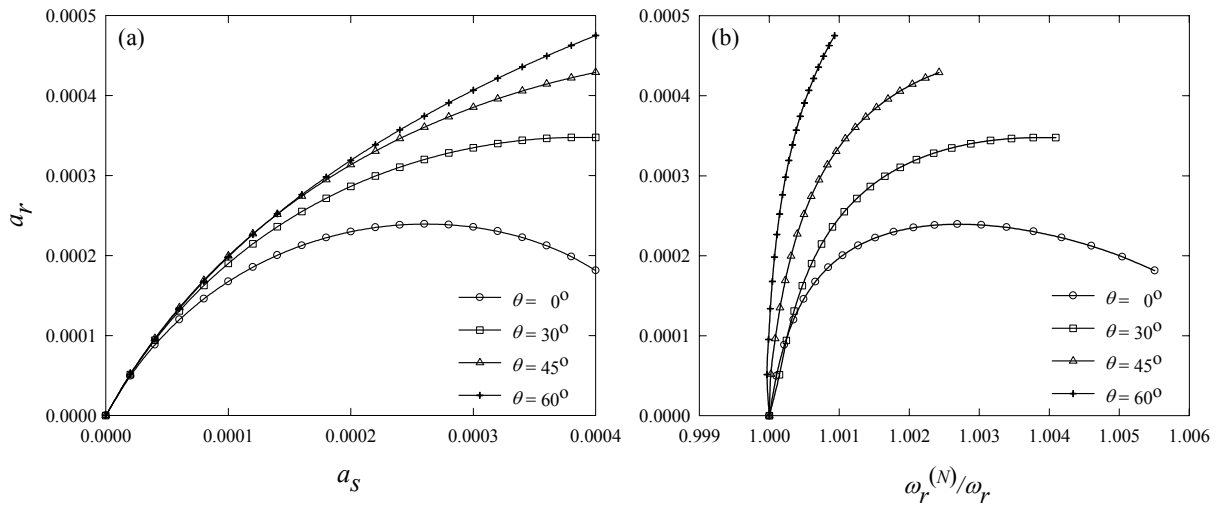


**Figure 6**

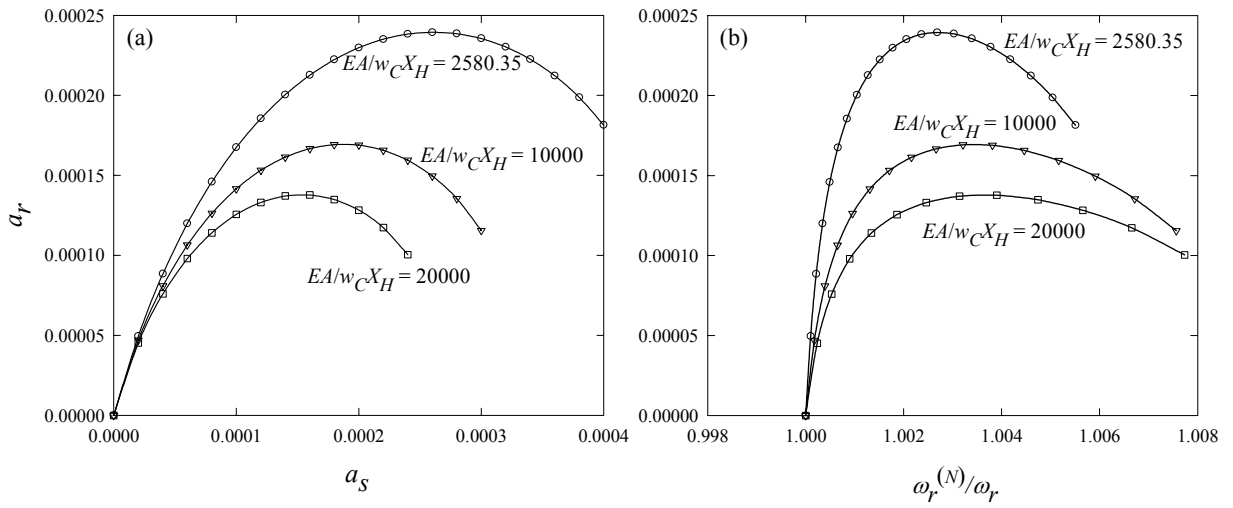


**Figure 7**

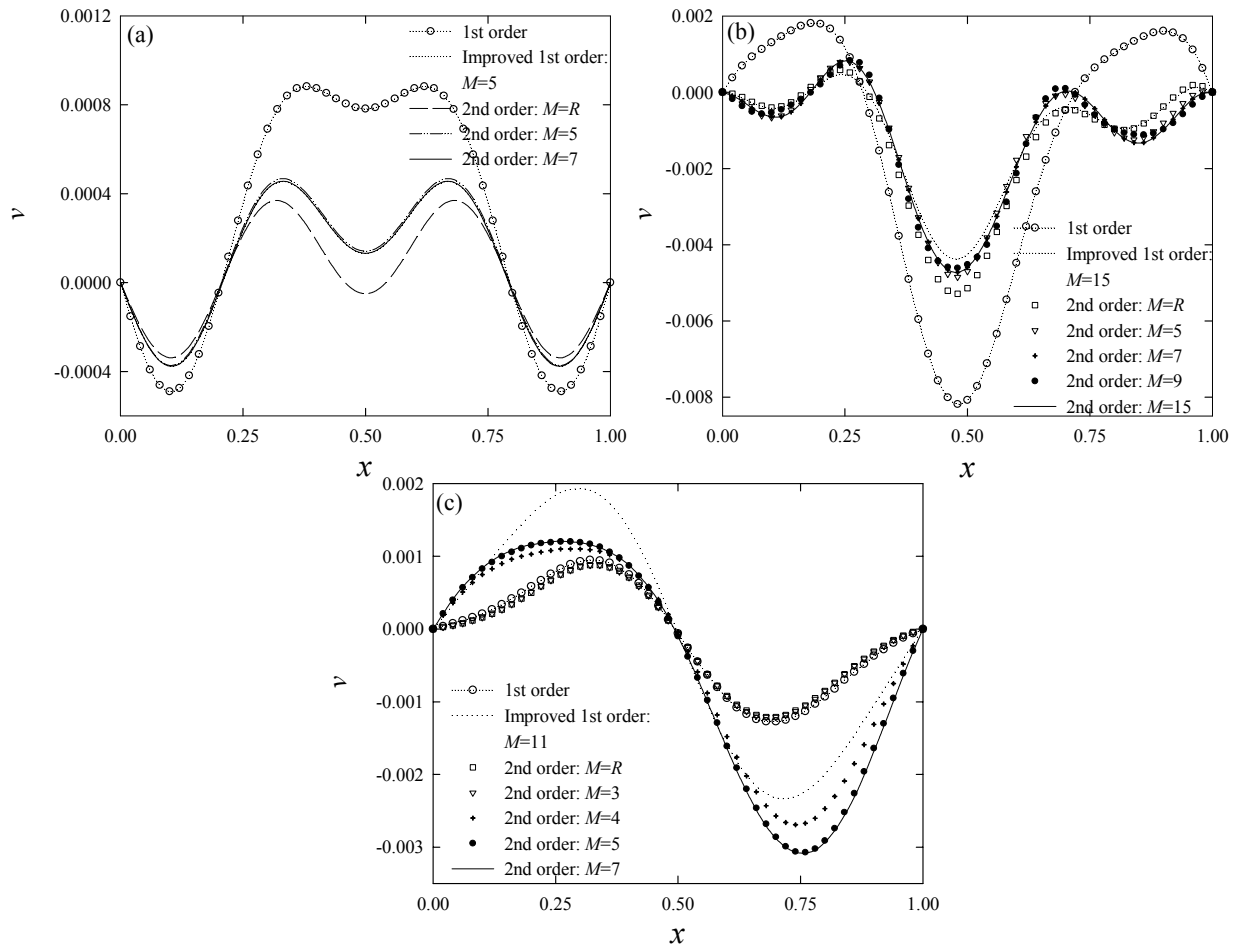


**Figure 8**

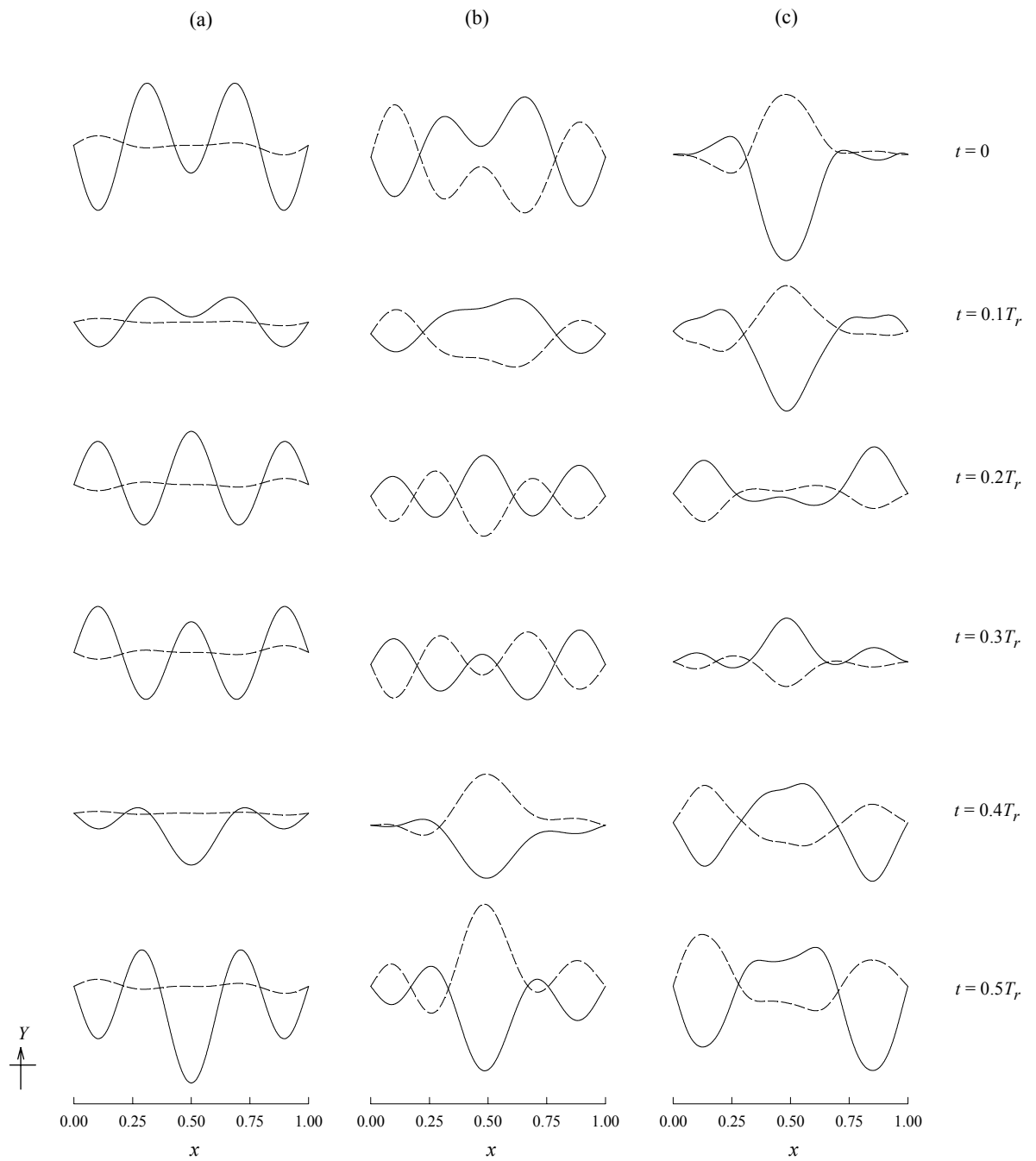


**Figure 9**

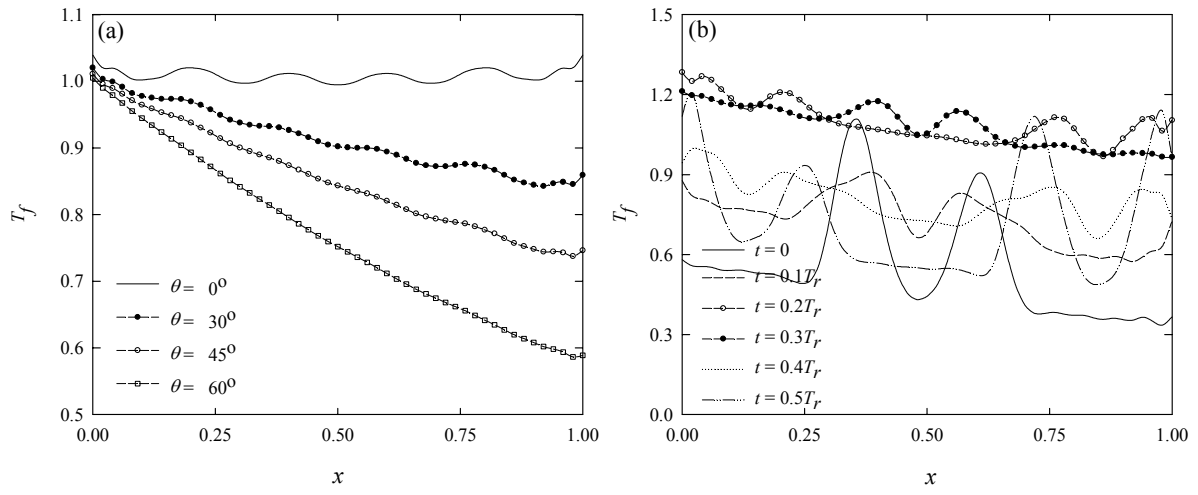


**Figure 10**

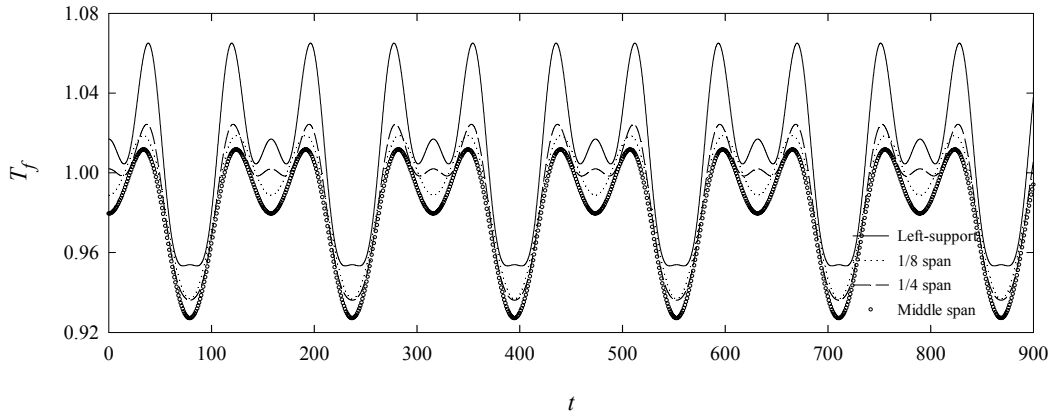


**Figure 11**

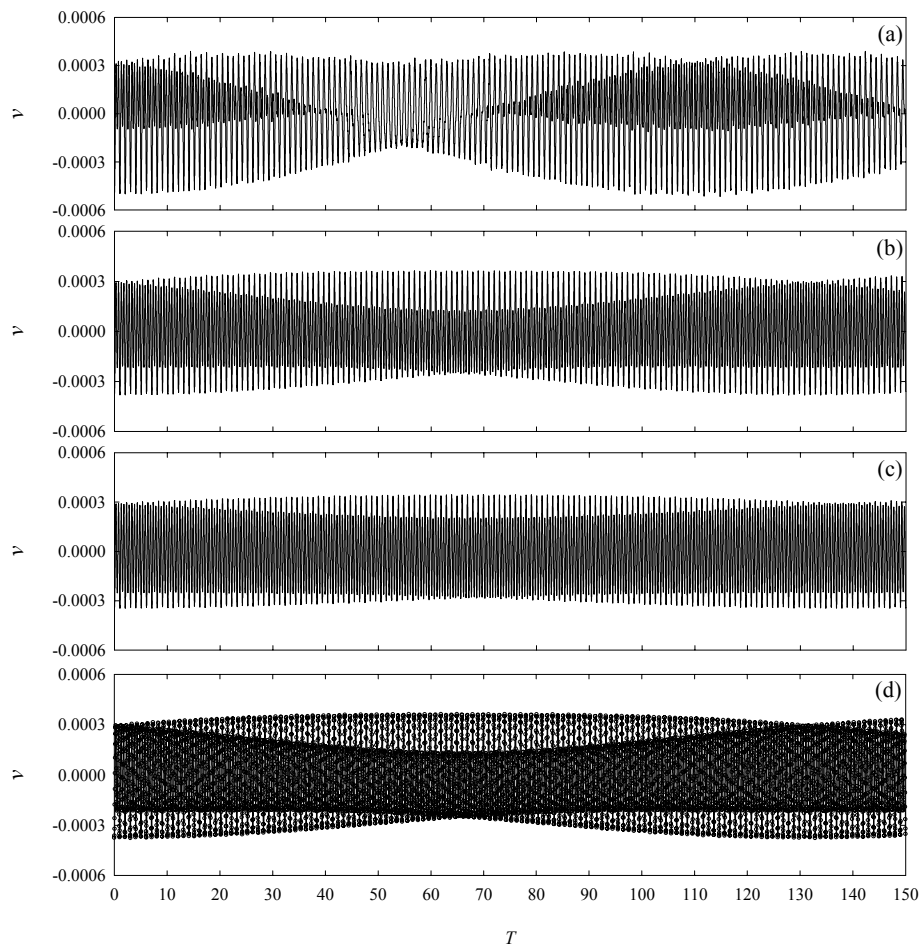


**Figure 12**

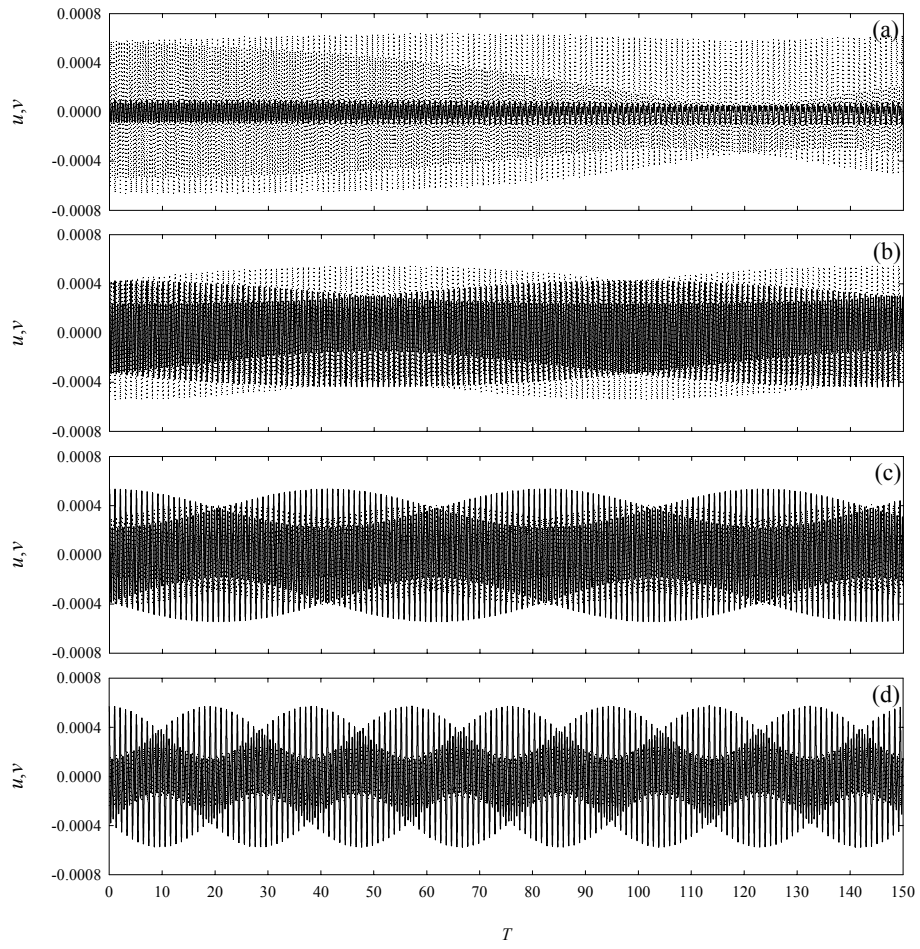


**Figure 13**

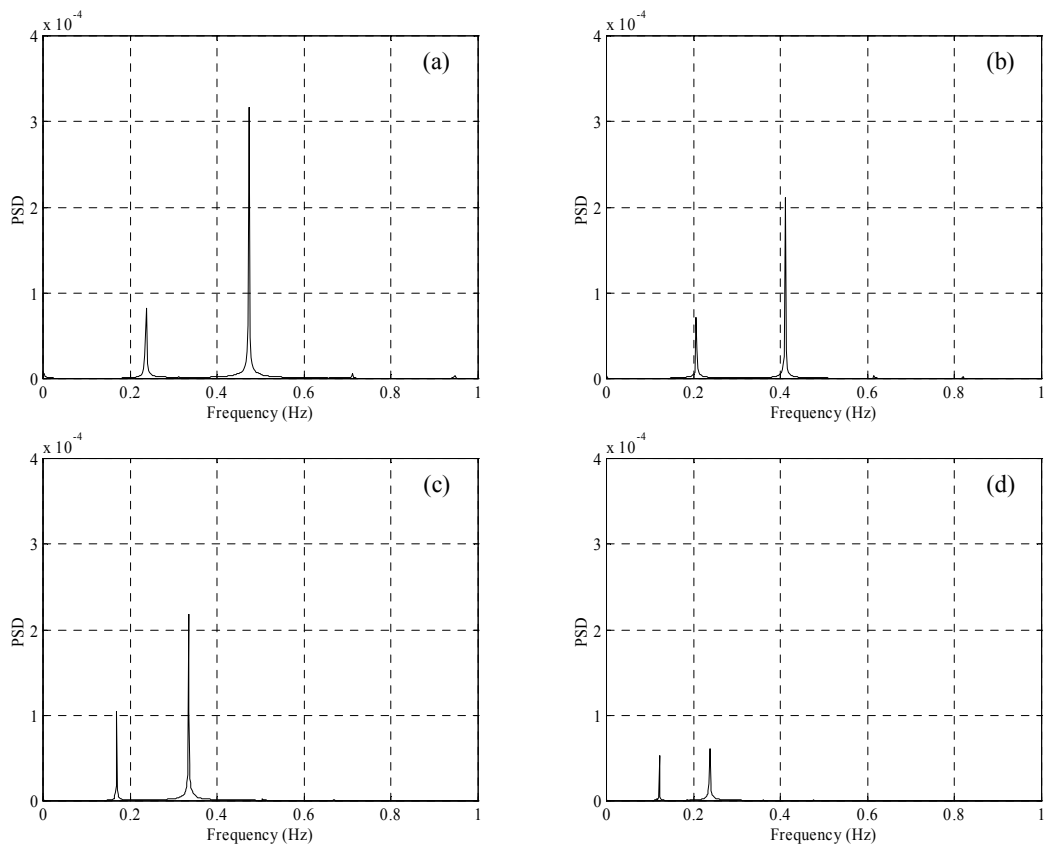


**Figure 14**

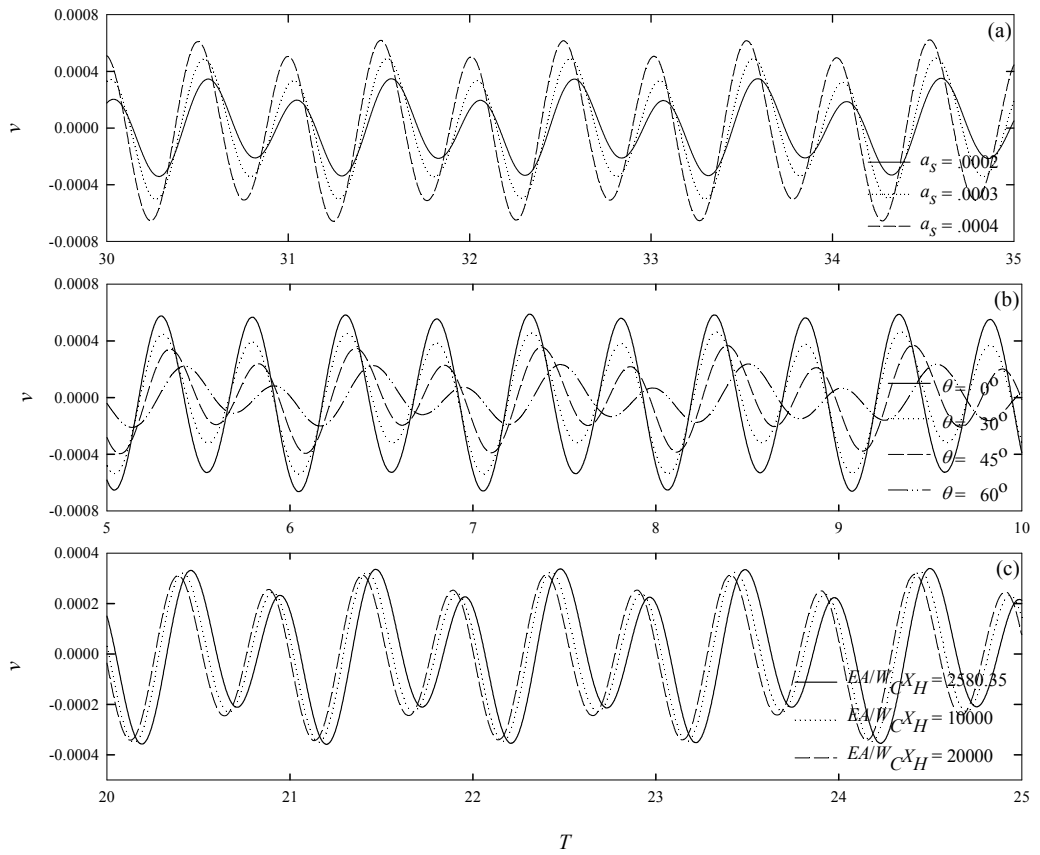


**Figure 15**



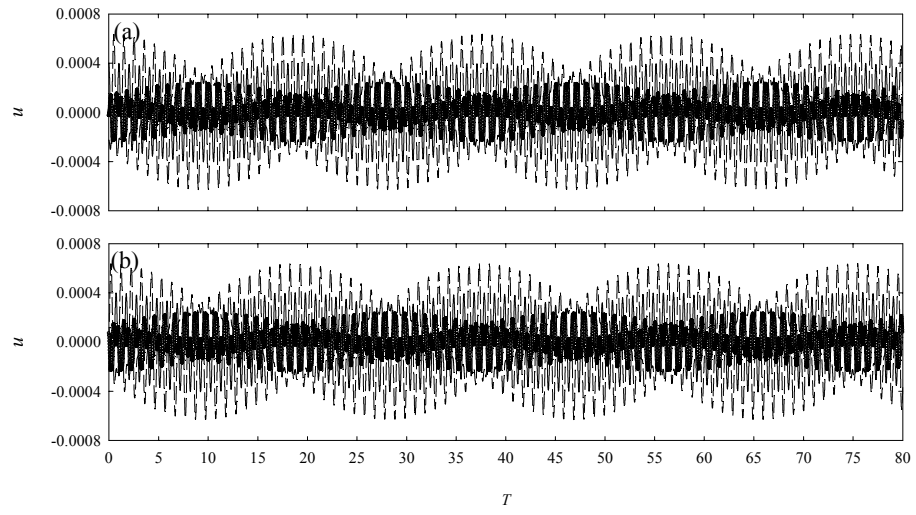


**Figure 16**

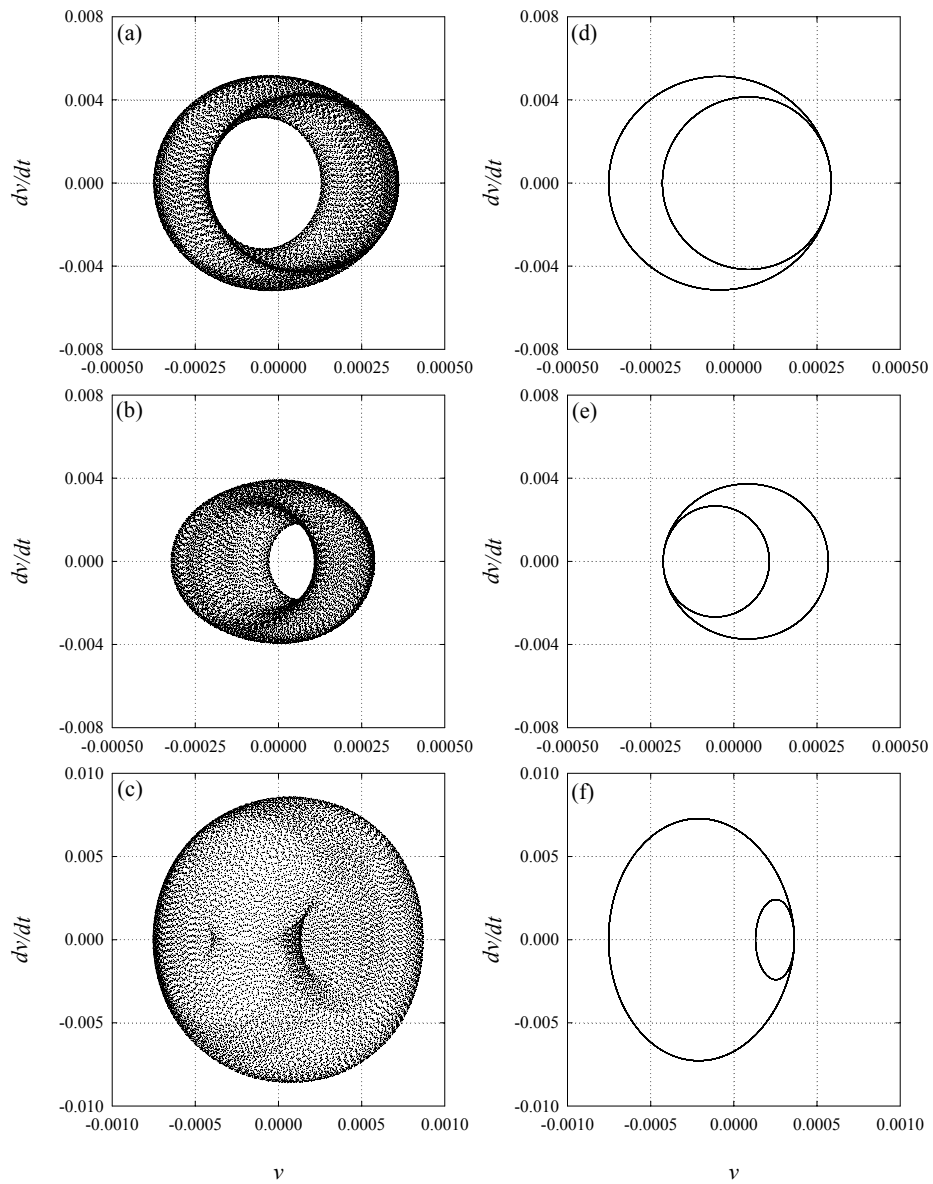


**Figure 17**

**Table 1**

$\lambda/\pi$	$\alpha$	$d$	$r-s$	$\omega_r$	$\omega_s$	$\Re$		
			Order (Mode*)			NC		CC
						$\rho \neq 1$	$\rho \approx 1$	
1.28	475.7	.023	1(S)-3(S)	4.76	9.51	465.733	453.730	448.991
2	640.6	.031	1(A)-4(A)	6.26	12.55	0	0	0
			2(S)-4(A)	6.28	12.55	0	0	0
2.95	828.2	.040	2(S)-5(S)	7.91	15.82	1210.677	1419.739	1432.430
3.23	878.1	.043	3(S)-7(S)	10.94	22.03	3071.039	3092.333	3189.458
4	1013.5	.049	1(A)-3(S)	6.22	12.48	-12265.279	-12534.834	-12851.058
			1(A)-4(A)	6.22	12.54	0	0	0
5.48	1246.7	.060	2(S)-5(S)	8.82	17.57	-31316.003	-31928.934	-31744.898

\* S (A): symmetric (anti-symmetric)

**Table 2**

$\lambda/\pi$	$\theta$	$\alpha$	$d$	$r-s$	$\omega_r$	$\omega_s$	$\Re$
1.28	30°	548.6	.031	1-3	4.42	8.84	312.729
2.95	30°	955.6	.053	2-5	7.36	14.70	959.154
	45°	1170.8	.080	2-5	6.70	13.30	494.389
	60°	1655.5	.161	2-5	5.73	11.22	115.426
3.23	30°	1014.3	.057	3-7	10.16	20.46	-2144.941
3.84	30°	1137.5	.064	1-4	5.75	11.72	3231.275
4.14	30°	1195.7	.067	1-3	5.75	11.51	-4297.997
				1-4	5.75	11.97	7513.074
5.48	30°	1439.0	.080	2-5	8.19	16.26	-21348.404

**Table 3**

$m$	Modal contributions (%)					
	$\theta = 0^\circ$			$\theta = 30^\circ$		
	$K_{rr}^Q$	$K_{ss}^Q$	$K_{rs}^Q$	$K_{rr}^Q$	$K_{ss}^Q$	$K_{rs}^Q$
1 ( $r$ )	98.476	74.014	76.771	98.559	73.776	76.794
2	0	0	0	0.007	0.346	-0.047
3 ( $s$ )	1.308	26.009	23.119	1.214	25.886	23.267
4	0	0	0	0.012	0.015	-0.056
$M=5$	0.216	-0.023	0.110	0.209	-0.023	0.042

**Table 4**

$m$	Modal contributions (%)					
	$\theta = 0^\circ$			$\theta = 30^\circ$		
	$K_{rr}^Q$	$K_{ss}^Q$	$K_{rs}^Q$	$K_{rr}^Q$	$K_{ss}^Q$	$K_{rs}^Q$
1	0	0	0	0.328	0.337	-0.717
2 ( $r$ )	35.134	2.131	-6.673	32.805	2.293	-8.105
3	0	0	0	0.433	1.148	-2.091
4	-3.345	15.818	-22.223	-3.229	11.446	-18.826
5 ( $s$ )	56.672	81.280	137.184	51.519	84.329	138.869
6	0	0	0	7.497	0.424	-1.536
7	9.650	2.528	-10.053	8.806	1.972	-9.398
8	0	0	0	0.110	0.062	-0.787
9	1.268	0.033	1.850	1.144	0.028	2.517
10	0	0	0	0.021	-0.033	0.044
11	0.381	-2.042	-0.010	0.342	-2.343	0.067
:	:	:	:	:	:	:
$M=15$	0.080	0.067	-0.032	0.071	0.069	-0.021

**Table 5**

$m$	Modal contributions (%)					
	$\lambda/\pi = 3.84^a$			$\lambda/\pi = 4.14^b$		
	$K_{rr}^Q$	$K_{ss}^Q$	$K_{rs}^Q$	$K_{rr}^Q$	$K_{ss}^Q$	$K_{rs}^Q$
<sup>a,b</sup> 1( $r$ )	-0.670	0.150	2.162	0.528	0.013	2.868
2	-2.446	6.998	12.911	1.625	3.643	8.943
<sup>b</sup> 3 ( $s$ )	110.895	25.124	45.217	4.607	86.348	53.094
<sup>a</sup> 4 ( $s$ )	-2.844	64.530	32.006	86.348	8.930	29.140
5	-4.326	3.079	6.541	6.159	0.957	4.841
6	-0.036	0.008	0.055	0.053	0.003	0.149
7	-0.397	-0.293	0.752	0.482	-0.171	0.660
8	-0.006	-0.256	0.009	0.007	0.016	0.005
9	-0.102	0.483	0.208	0.116	0.185	0.179
:	:	:	:	:	:	:
$M=15$	-0.009	0.022	0.019	0.010	0.010	0.017

**Table 6**

(a)			
$\theta$	$K_{rr}$		
	$K_{rr}^Q$	$K_{rr}^C$	$\Sigma$
0°	3380245.348	-2443516.680	936728.668
30°	1918638.007	-1405070.502	513567.505
45°	891003.539	-705675.662	185327.877
60°	241233.251	-230468.875	10764.376
(b)			
$\theta$	$K_{ss}$		
	$K_{ss}^Q$	$K_{ss}^C$	$\Sigma$
0°	43656384.761	-109638064.379	-65981679.618
30°	24731628.708	-61808123.938	-37076495.229
45°	11127469.293	-28054512.094	-16927042.801
60°	2886187.962	-7461794.632	-4575606.670
(c)			
$\theta$	$K_{rs}$		
	$K_{rs}^Q$	$K_{rs}^C$	$\Sigma$
0°	10538434.283	-21960899.470	-11422465.188
30°	5918207.453	-12468727.488	-6550520.035
45°	2677493.735	-5945924.924	-3268431.189
60°	698677.986	-1754799.169	-1056121.184